Electrochimica Acta 457 (2023) 142404

Contents lists available at ScienceDirect

Electrochimica Acta

journal homepage: www.journals.elsevier.com/electrochimica-acta

Pitting corrosion on highly alloyed stainless steels in dilute sulphuric acid containing sodium chloride

E. Huttunen-Saarivirta [a,*], E. Isotahdon [a], Z. Que [a], M. Lindgren [b], A. Mardoukhi [b], J.-B. Jorcin [c], P. Mocnik [d], T. Kosec [d], Y. El Ouazari [e], S. Hägg Mameng [e], L. Wegrelius [e]

[a] VTT Technical Research Centre of Finland Ltd, P.O. Box 1000, FI-02044 VTT, Finland
[b] Metso Outotec Research Center, P.O. Box 69, FI-28101 Pori, Finland
[c] Tecnalia, Parque Cientifico y Tecnologico de Bizkaia, Derio, Spain
[d] ZAG Slovenian National Building and Civil Engineering Institute, Dimičeva ulica 12, Ljubljana, SI 1000, Slovenia
[e] Outokumpu Stainless AB, Box 74, SE-77422 Avesta, Sweden

ARTICLE INFO

Keywords:
Stainless steel
Austenitic
Duplex
Pitting attack
Passivity breakdown

ABSTRACT

Stainless steels are widely used in industrial assets and equipment. Despite their good corrosion resistance under a wide range of operating conditions, there is the possibility of pitting corrosion in the presence of chlorides. However, very few studies have identified the safe operating conditions for various high-alloyed stainless steel grades by comparing their pitting susceptibility. In this research, the susceptibility to pitting attack of five stainless steels with austenitic and duplex microstructures was examined in dilute sulphuric acid solution with varying amounts of NaCl at the temperatures of 50, 90 and 130°C. Based on potentiodynamic polarization scans, none of the test materials underwent pitting corrosion at 50°C, but differences in susceptibility to pitting attack were clear between the test materials and NaCl concentrations at the temperature of 90°C, and further temperature increase facilitated uniform corrosion. 28-day immersion tests at 90°C confirmed the pitting susceptibility of duplex grades 1.4662 (PREN 33) and 1.4462 (PREN 35) in the presence of at least 2000 mg/L NaCl, but not the susceptibility of a corresponding austenitic grade 1.4539 (PREN 34). The grades 1.4547 (PREN 43) and 1.4410 (PREN 44) were not susceptible to pitting corrosion under any of the studied conditions. The results from materials microstructural and electrochemical characterization are presented and discussed in this paper.

1. Introduction

Stainless steels are iron-based alloys, in which the chromium content is high enough to introduce the evolution of a thin protective layer of Cr_2O_3 on the surfaces, a phenomenon called passivity [1,2]. Although 12 wt.% chromium in the alloy makes it "stainless", it is known that the corrosion resistance of stainless steels improves with an increase in the chromium content [1]. The alloying defines not only the passive film development and characteristics, but also the material microstructure. Stainless steels with austenitic microstructure are typically easily weldable and show excellent ductility and corrosion resistance over a wide range of conditions, thus they are common construction materials for demanding industrial conditions. Ferritic grades, in turn, may undergo a ductile-brittle transition, which challenges their use under mechanical loads and as thick sections, while martensitic grades are characterized by the combination of a high hardness and high strength, and slightly compromised weldability, overall ductility and corrosion resistance [1,3,4]. Furthermore, duplex ferritic-austenitic grades combine many of the attractive properties of the austenitic and ferritic microstructures at reasonable costs: they feature high strength, good low-temperature toughness, and greater resistance to stress corrosion cracking and hydrogen embrittlement as compared to single-phase austenitic and ferritic counterparts. Duplex stainless steels also find use under harsh operating conditions, being thus considered as viable substitutes for the austenitic grades [5]. However, no research effort has been put on systematically comparing the susceptibility to localized corrosion, in particular pitting corrosion that is of vital practical importance in many industrial applications, in austenitic and duplex stainless steels.

To respond to the growing demand for metals, hydrometallurgical processing of mineral raw materials has become increasingly important due to lower energy and water demand as compared to

* Corresponding author.
E-mail address: elina.huttunen-saarivirta@vtt.fi (E. Huttunen-Saarivirta).

https://doi.org/10.1016/j.electacta.2023.142404
Received 4 November 2022; Received in revised form 11 April 2023; Accepted 11 April 2023
Available online 14 April 2023

Table 1
Stainless steel grades included in the research.

Designation		Alloying, wt.%									Microstructure
EN	UNS	PREN	Cr	Ni	Mo	N	C	Mn	Si	Others	
1.4662	S82441	33.4	23.87	3.59	1.66	0.256	0.024	2.84	0.43	0.32 Cu	Duplex
1.4539	N08904	34.3	19.62	24.03	4.23	0.049	0.011	1.34	0.31	1.35 Cu, 0.31 Co	Austenitic
1.4462	S32205	35.4	22.24	5.84	3.18	0.166	0.016	1.34	0.35	0.31 Cu, 0.19 Co	Duplex
1.4547	S31254	42.8	19.76	17.79	6.05	0.192	0.016	0.53	0.37	0.65 Cu	Austenitic
1.4410	S32750	43.8	25.69	7.18	3.96	0.312	0.012	0.78	0.43	0.31 Cu	Duplex

Table 2
Test conditions in the electrochemical measurements. The equilibrium data are obtained using HSC Chemistry 10 software [30]. The results for the highest NaCl (10000 mg/L) at 130°C are not presented in the paper due to instability of the system due to very high corrosion rate, therefore the values are in parentheses.

Electrolyte		**Temperature of 50 °C**			**Temperature of 90 °C**			**Temperature of 130 °C**		
H_2SO_4 wt.%	NaCl, mg/L	$a(Cl^-)$	$a(Cl^-)/\ a(SO_4^{2-})$	Calculated pH	$a(Cl^-)$	$a(Cl^-)/\ a(SO_4^{2-})$	Calculated pH	$a(Cl^-)$	$a(Cl^-)/\ a(SO_4^{2-})$	Calculated pH
1	0	0	0	1.04	0	0	1.09	0	0	1.12
	500	0.0001	1.7	1.05	0.0001	5.3	1.09	0.0001	19.1	1.12
	1000	0.0002	3.3	1.05	0.0002	10.3	1.09	0.0002	38.0	1.13
	2000	0.0005	6.7	1.05	0.0005	20.5	1.10	0.0004	74.9	1.13
	5000	0.001	16.8	1.06	0.001	50.3	1.11	0.001	181.3	1.15
	10,000	0.002	34.2	1.06	0.002	99.4	1.13	(0.002)	(351.8)	(1.17)

pyrometallurgical processes, and flexibility to raw material quality [6, 7]. Hydrometallurgy relies on extraction, in which metals from the minerals are dissolved as cations into the aqueous electrolyte, the common leachant being sulphuric acid. The extraction kinetics and efficiency may be improved by utilizing elevated temperature and oxidizing agents [8–11]; the latter may be intentionally added or co-dissolved together with the target metal cations as, e.g., Fe^{3+} or Cu^{2+}. Furthermore, chlorides (Cl^-) are typically included in the leachant, again either in purpose, because they contribute to cation speciation and the overall solution chemistry via complex formation [9,12,13], or from the raw materials. The aggressive nature of the operating environment is reflected to the materials selection: highly corrosion-resistant austenitic or duplex stainless steel grades are typical material candidates for the hydrometallurgical assets and equipment: tanks, containers, pipes, tubes, valves and mixers [14]. However, although it has been acknowledged that the corrosion performance of construction materials is of high importance [15–18], there is no performance data available to support proper stainless steel selection for hydrometallurgy applications. Therefore, in order to ensure the safety at hydrometallurgical process sites, it is essential to evaluate the corrosion risk of the construction materials.

Iso-corrosion diagrams that present a constant uniform corrosion rate for a specific material as a function of environmental variables (concentration, temperature) typically guide the material selection in pure chemicals, such as sulphuric acid [19]. They reveal that, e.g., austenitic alloy 1.4539 and duplex grades 1.4462 and 1.4410 can be used in dilute solutions. However, chlorides in the electrolyte may facilitate the localized breakdown of the passive film, hence the susceptibility of the material to pitting corrosion [20–23], particularly under oxidizing conditions aggravated in the presence of oxidizing species like Fe^{3+} and Cu^{2+}. Altpeter and Rockel [23] have conducted immersion experiments for the grade 1.4539 (and some higher alloyed austenitic stainless steel grades) in 5, 10, 20 and 50 wt.-% H_2SO_4 with the additions of 500 or 3000 ppm Cl^-, or 2000 ppm Cu^{2+}, at the temperatures of 50, 100 and 150°C. At 50°C, the corrosion rate of grade 1.4539 in the absence of Cl^- was 0.04 mm/year or lower at all studied H_2SO_4 concentrations. The presence of chlorides slightly accelerated the uniform corrosion, up to 0.17 mm/year in 20 wt.% H_2SO_4 at the content of 3000 ppm Cl^-. At 100°C, the uniform corrosion rate of the alloy was clearly higher than at 50°C, up to 2.4 mm/year in 20 wt.% H_2SO_4, and the presence of chlorides (500 and 3000 ppm Cl^-) slightly lowered the corrosion rate. No pitting corrosion was reported for grade 1.4539 in any of the test solutions. The influence of the presence of cuprous cations, Cu^{2+}, in the corrosion rate of grade 1.4539 was proved negligible. Consistently, Streicher [24] has demonstrated that oxidizing cations, such as Fe^{3+}, inhibit the uniform corrosion austenitic stainless steels 1.4301 and 1.4404 in concentrated acids, including boiling sulphuric acid. Laylock and Newman [25] have studied the pitting corrosion of austenitic stainless steels, including the grade 1.4539, in 1 M NaCl at the temperature of 50°C and beyond. Although no acid was included in the solution, the NaCl concentration was high enough to introduce pitting at all test temperatures. The breakdown potential was demonstrated to decrease almost linearly with an increase in temperature, at the average rate of −3.3 mV / °C. Liu and Wu [26] have examined the corrosion behaviour of grade 1.4547 in 3.5% NaCl solution within the pH range from 0.1 to 5.0, with the pH being adjusted by adding HCl. Their results revealed spontaneous passivation at the highest potentials and clear active-passive transition at pH values 3 and lower, but no pitting corrosion in any of the solutions. As for the duplex stainless steels, corrosion studies in sulphuric acid or other low-pH solutions with chlorides are even more fragmented. Tsai and Chen [27] have examined the stress corrosion cracking (SCC) behaviour of duplex grade 1.4662 in near-neutral (pH=6) concentrated NaCl solution at 90°C. Their results showed that SCC occurred around the breakdown potential through a pitting corrosion-assisted mechanism; hence at high enough NaCl concentrations the alloy undergoes pitting despite the near-neutral pH value. The work by Garfias-Mesias et al. [28] has focussed on the pitting corrosion in super duplex grade 1.4507 after annealing for 2 h at various temperatures. Critical pitting temperature was defined in $FeCl_3$ solutions, and it was the lowest in the case where the ferrite fraction in the microstructure was the highest. Indeed, the pitting attack was shown to occur preferentially in the ferrite phase.

Based on the above, it is evident that in pure sulphuric acid solutions, uniform corrosion is the dominant corrosion form for austenitic and duplex stainless steels. With increase in the chloride content of the solution, the type of attack changes into pitting corrosion, which is much more challenging for the integrity of the industrial equipment. Additionally, very few studies have identified the safe operating conditions for various stainless steel grades by systematically comparing their pitting susceptibility as a function of environmental conditions, such

Table 3
Conditions in the immersion experiments.

Materials	Solution #	H_2SO_4 content, wt.%	SO_4^{2-} addition, mg/L	NaCl, mg/L	$a(Cl^-)/a(SO_4^{2-})$	Addition of cations, mg/L
1.4539	1	1	–	500	5	–
1.4462, 1.4539	2	1	–	1000	10	–
1.4462, 1.4662, 1.4539, 1.4410, 1.4547	3	1	–	2000	20	–
1.4462, 1.4662, 1.4410, 1.4547	4	1	–	5000	49	–
1.4539	5	1	–	500	3.7	Fe^{3+}, 500
1.4539	6	1	–	500	0.7	Fe^{3+}, 5000
1.4462, 1.4539	7	1	–	1000	7.5	Fe^{3+}, 500
1.4462, 1.4539	8	1	–	1000	1.4	Fe^{3+}, 5000
1.4539	9	1	20,000	1000	1	Fe^{3+}, 5000
1.4462	10	1	–	1000	3.3	Cu^{2+}, 5000
1.4462	11	1	–	1000	2.6	Fe^{2+}, 5000
1.4662, 1.4410	12	1	–	2000	14.9	Fe^{3+}, 500
1.4462, 1.4662, 1.4539, 1.4410, 1.4547	13	1	–	2000	2.8	Fe^{3+}, 5000
1.4539	14	1	20,000	2000	2.2	Fe^{3+}, 5000
1.4410	15	1	–	2000	6.6	Cu^{2+}, 5000
1.4410	16	1	–	2000	5.2	Fe^{2+}, 5000
1.4462	17	1	20,000	2000		Fe^{2+}, 5000
1.4662	18	1	–	5000	37	Fe^{3+}, 500
1.4462, 1.4662, 1.4410, 1.4547	19	1	–	5000	7.1	Fe^{3+}, 5000
1.4662, 1.4410	20	1	20,000	5000	5.0	Fe^{3+}, 5000
1.4410	21	1	–	5000	16.3	Cu^{2+}, 5000

chloride concentration and temperature. This paper aims to bridge this knowledge gap and, by doing so, also provide an understanding of the role of material microstructure in initiating the attack in tests environments representative of hydrometallurgical processes. The work involves five stainless steels: two austenitic and three duplex grades with the pitting resistance equivalent number (PREN) between 33 and 44.

2. Experimental

2.1. Materials and solutions

Five grades of stainless steel were studied: the duplex grades of EN 1.4462, EN 1.4662, and EN 1.4410, and the austenitic grades of EN 1.4539 and EN 1.4547. The actual compositions of the grades together with the PREN values calculated according to [21]:

$$\mathrm{PREN} = \%\mathrm{Cr} + 3.3\mathrm{x}\%\mathrm{Mo} + 16\mathrm{x}\%\mathrm{N} \quad (1)$$

are given in Table 1. The test materials were supplied by Outokumpu Stainless AB, Sweden. The surfaces of the specimens were wet ground to the 320 grit surface finish, ultrasonically cleaned in acetone, rinsed with ethanol, dried, and then let to oxidize in the atmospheric air for at least 18 h.

The chemistry of electrolytes in electrochemical measurements was selected according to the sulphuric acid and chloride ion concentrations of hydrometallurgical processes. Further, based on our earlier results for stainless steel grades with lower PREN values [20] and preliminary results collected for the five grades of interest, the sulphuric acid concentration of 1% was used in the tests. The solution was added with varying amounts of NaCl, up to 10,000 mg/L, Table 2. Chemicals of analytical grade purity and ion-exchanged water were used to prepare test solutions. The equilibrium data at the temperatures relevant for the work were calculated using HSC Chemistry 10 software [29]. Chloride concentrations varied from 300 to 6000 mg/L, with chloride activities in equilibrium, $a(Cl^-)$, in the range from 0.0001 to 0.0020 independently of the test temperature. Equilibrium sulphate concentrations and, hence, sulphate activities, $a(SO_4^{2-})$, showed a strong temperature dependency, yielding the ratio of chloride and sulphate activities, $a(Cl^-)/a(SO_4^{2-})$, in the range from 1.7 up to 181. Calculated pH values fell within the range of 1.0 to 1.2.

The electrolyte in the immersion tests had the sulphuric acid content of 1 wt.%, with the concentration of chlorides, Cl^-, metal cations: Fe^{3+}, Fe^{2+} or Cu^{2+}, and sulphates, SO_4^{2-}, varied. Table 3 summarizes the chemistry of the used electrolytes. Altogether, 21 different solution chemistries were used, enabling to evaluate the influence of chloride concentration, the presence of metal cations and, in the case of Fe^{3+}, their content, and the activity ratio of chlorides to sulphides, $a(Cl^-)/a(SO_4^{2-})$. Chlorides were added in 1 wt.% sulphuric acid solution as NaCl, while metal cations were included as the following sulphates: Fe^{3+} as $Fe_2(SO_4)_3$, Fe^{2+} as $FeSO_4$, and Cu^{2+} as $CuSO_4$. In some of the solutions, additional SO_4^{2-} was introduced as Na_2SO_4 (#9, #14, #17 and #20). All immersion experiments were performed at 90°C, thus the prepared solutions were heated either in a heating cabinet or using a hot plate before the specimens were immersed in them.

2.2. Electrochemical measurements

Electrochemical measurements for the test materials were performed at three temperatures: 50°C, 90°C and 130°C (Table 2). The measurements at 50°C and 90°C were performed in an electrochemical glass cell with double walls, enabling maintaining the desired temperature via circulating hot water/oil heated by an external unit. The counter electrode was either a platinum grit or a glassy carbon electrode, while Ag/AgCl electrode in saturated KCl solution, and at 90°C with a salt bridge, was used as a reference electrode. The studied plate specimen was located in the bottom of the cell with the help of flat rubber gaskets (that did not yield crevice corrosion, in contrast to conventional Avesta cell). The exposed area of the working electrode was 1–2 cm^2, with the electrolyte volume being approximately 0.35 L. The measurements at 130°C were carried out in a Cormet Hastelloy C276 autoclave using cylindrical specimens of 15 mm in height and 10 mm in diameter. A wire of grade 1.4404 (316 L) stainless steel was carefully welded on each cylinder to provide an electrical contact so as to avoid the propagation of the heat-affect zone in the material, after which the weld area and the connector wire were covered by a Teflon sheath. The exposed area of the material of interest (the casing and bottom) was 3.2–4.5 cm^2, with the electrolyte volume being 1 L. Prior to the tests, the electrolyte was warmed to the test temperature with an external resistance jacket. The autoclave tests employed platinum as a counter electrode and a silver-silver chloride (Ag/AgCl-saturated KCl) electrode as a reference electrode. In the following, all measurements are reported against Ag/AgCl reference electrode (potential $E = 0.210$ V at 22 °C).

The electrochemical measurements involved open circuit potential (OCP) measurements and cyclic potentiodynamic polarization measurements. In all cases, the electrolyte was purged with nitrogen gas (N_2)

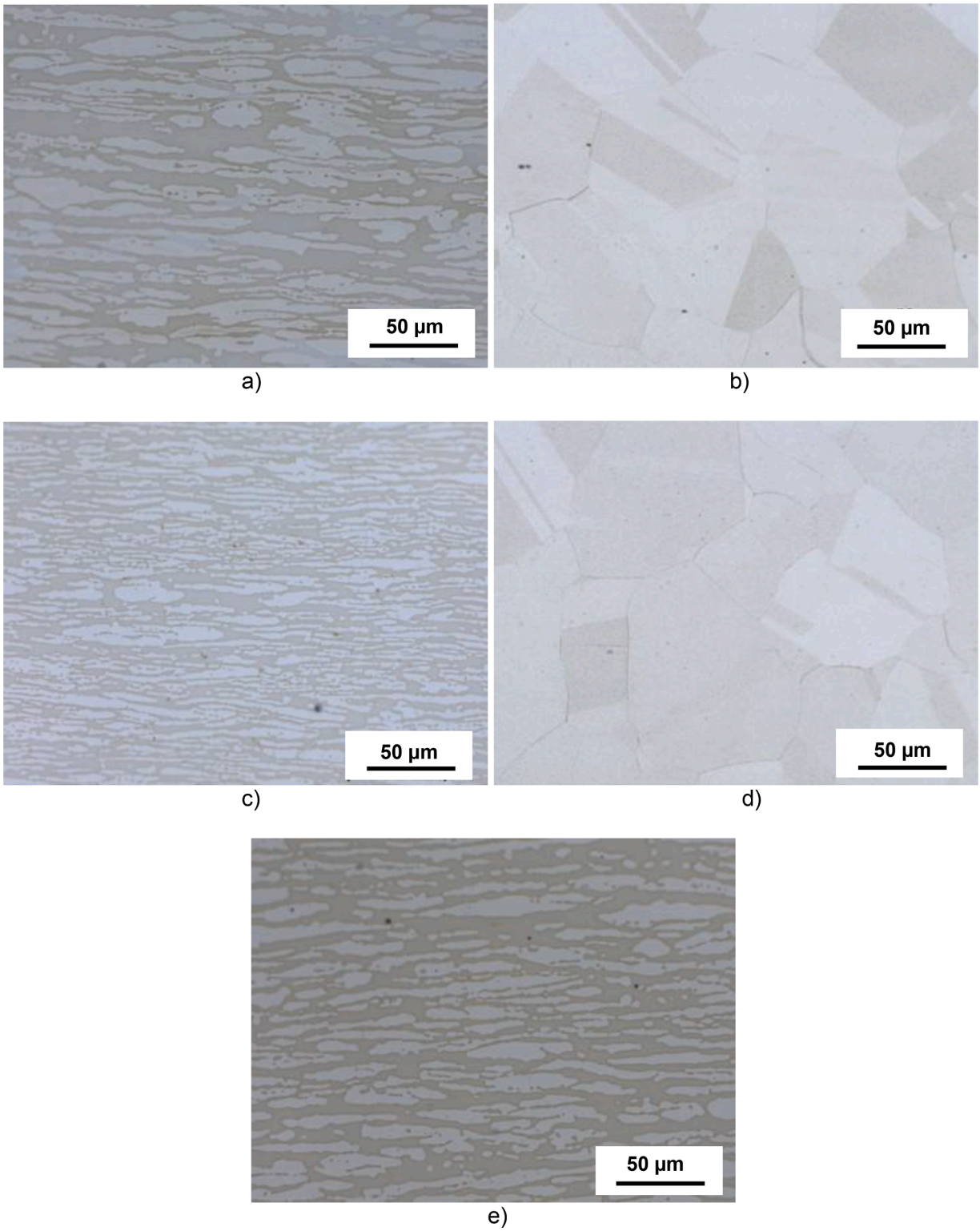

Fig. 1. Optical micrographs, showing the cross-sectional microstructure of the studied stainless steel grades. a) 1.4662, b) 1.4539, c) 1.4462, d) 1.4547, e) 1.4410.

before and during the measurements, in order to remove dissolved air. In addition to purging the test solution with N_2 in the 130°C experiments, the autoclave was closed and filled with N_2 up to 5 bars and then released, the cycle, which was repeated at least five times to deaerate the autoclave and ensure that there was no leakage. The electrochemical measurements under each set of test conditions were performed sequentially for one specimen. First, OCP measurements were performed for at least 1 hour or until OCP stabilized ($\Delta E/\Delta t$ was less than 20 mV/20 min). OCP measurements were then followed by cyclic potentiodynamic polarization measurements that were conducted from the cathodic potential of −0.25 V vs. OCP up to the anodic value of +1.4 V at a scan rate of 0.167 mV/s. The cut-off current density value of 0.1 mA/cm^2 was defined for the measurements. The measurements were performed using either a Gamry Reference 600 or a Princeton Applied

Table 4
Typical composition in wt.% of the ferrite (body-centred cubic, BCC) and austenite (face-centred cubic, FCC) phases included in the studied duplex stainless steel grades based on ThermoCalc [32].

	Temp. °C	Phase	%	Cr	Ni	Mo	N	C	Mn	Si	Fe	PREN
1.4662	1080	BCC	51	25.5	2.9	2.0	0.06	0.006	2.8	0.5	66.4	33.1
		FCC	49	22.7	4.4	1.2	0.49	0.034	3.2	0.4	67.6	34.5
1.4462	1080	BCC	49	24.3	4.3	3.9	0.04	0.006	1.4	0.4	65.6	37.8
		FCC	51	20.6	7.0	2.5	0.29	0.030	1.6	0.4	67.7	33.5
1.4410	1120	BCC	51	26.3	5.3	4.6	0.08	0.005	0.6	0.3	62.8	42.8
		FCC	49	23.7	8.1	3.0	0.49	0.026	0.8	0.3	63.7	41.4

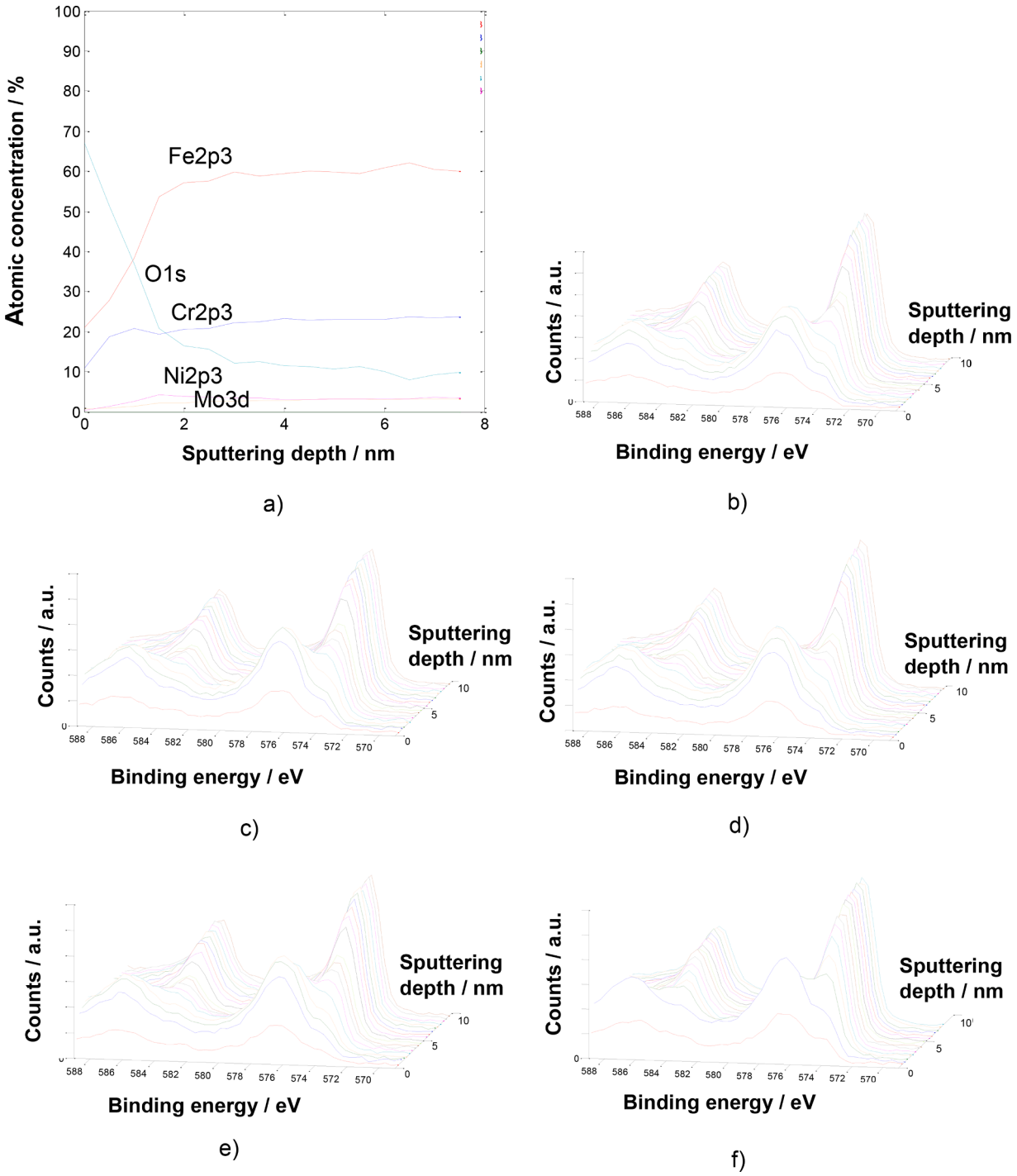

Fig. 2. XPS spectra for the test materials. a) Depth profile for the detected elements for grade 1.4410, sputtering rate 1 nm/min. Cr depth profiles for b) 1.4662, c) 1.4539, d) 1.4462, e) 1.4547, f) 1.4410. z-axis represents the sputtering depth, with the inter-spectral distance being 0.5 nm.

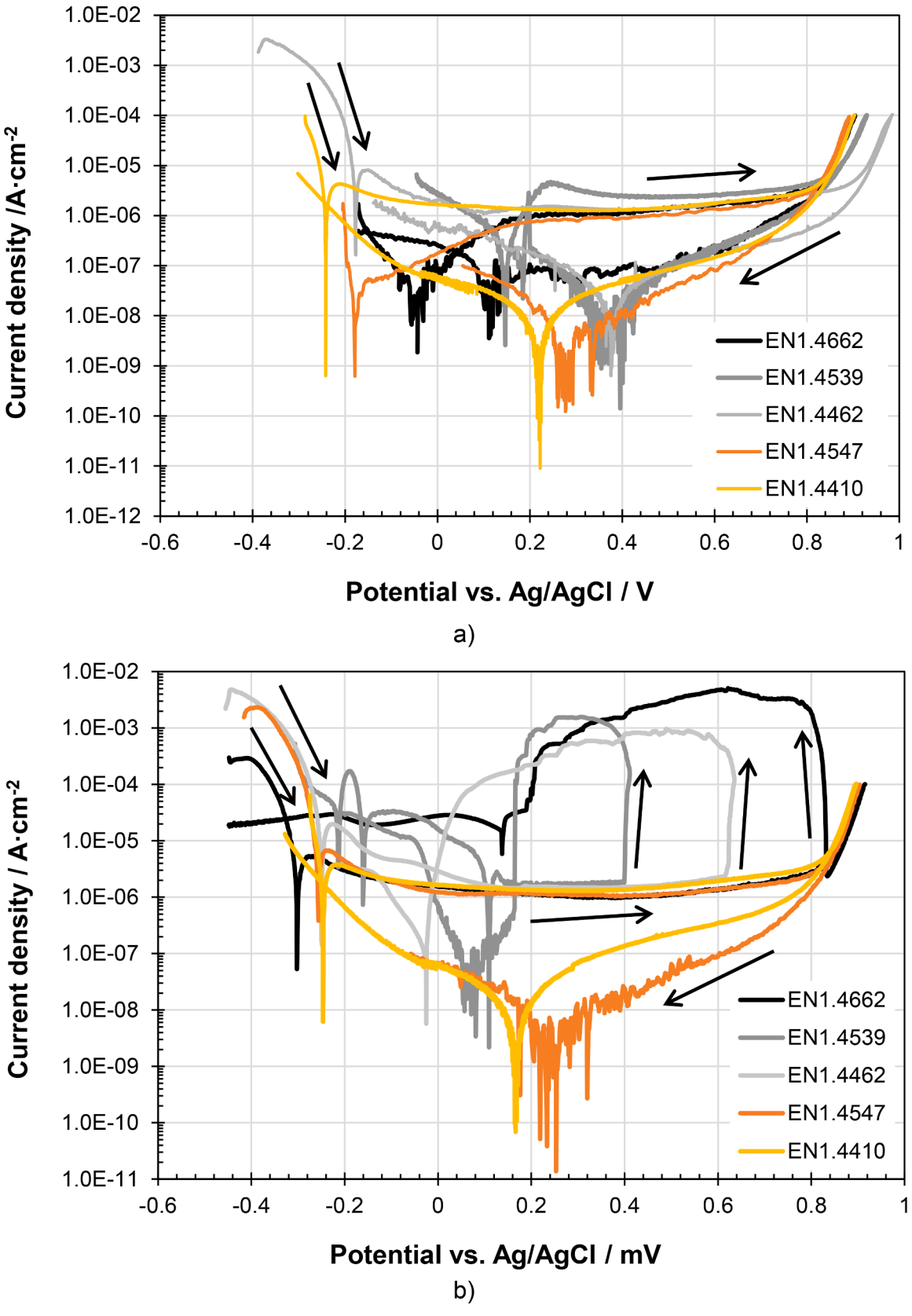

Fig. 3. Examples of potentiodynamic polarization curves for the five stainless steel grades in 1 wt.% H_2SO_4 at 90°C at two NaCl concentrations. a) 0 mg/L. b) 5000 mg/L. Black solid arrows indicate the scanning direction.

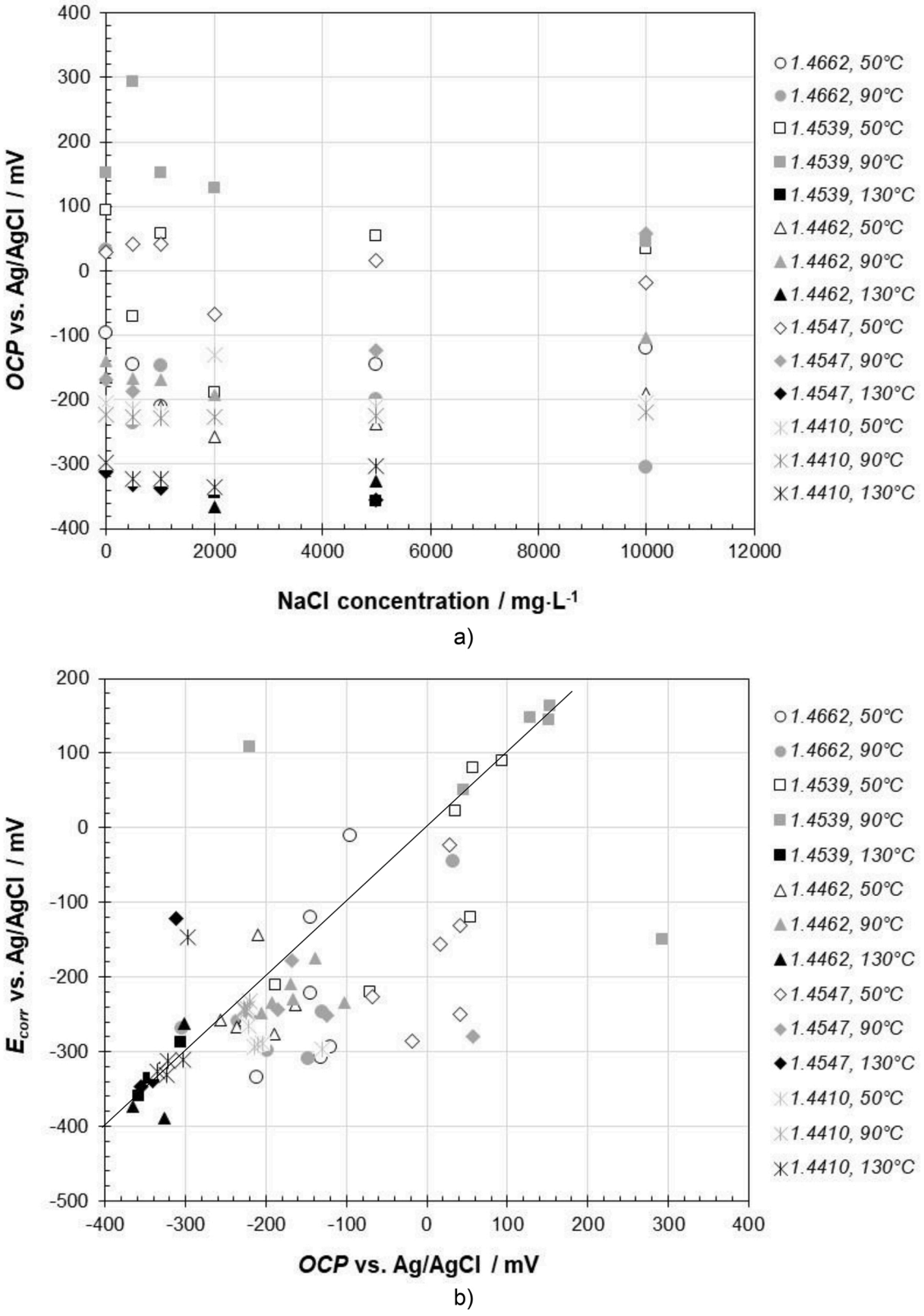

Fig. 4. a) Open circuit potential (OCP) values and b) correlation between corrosion potential, E_{corr}, and OCP for the alloys at the three test temperatures.

Research VersaSTAT 3 potentiostat, and the data was analysed with the related analysis software. In each case, the following electrochemical parameters related not only to pitting corrosion but also overall corrosion behaviour were extracted from the measurement data: OCP in the end of the measurement period, corrosion potential (E_{corr}) and corrosion current density (i_{corr}) that were extrapolated from Tafel fits, critical passivation current density (i_{crit}), passivation potential (E_{pass}), passive current density (i_{pass}), and breakdown potential (E_b). Where a positive hysteresis was detected in the cyclic potentidynamic curve, also repassivation potential (E_{rep}) was defined. Finally, corrosion rate (CR) was

calculated from i_{corr} according to Faraday's law. The reliability of the results was verified by checking the consistency of observed trends. Where the positive hysteresis was detected in the cyclic potentiodynamic curve, at least two parallel measurements (often more) were run (with the average values being presented).

2.3 Immersion tests

For the immersion experiments, specimens with the surface area of at least 20 cm^2 were used, following [30]. The dimensions of the specimens slightly varied between the steel grades, being either 40 mm x 25 mm, 50 mm x 20 mm or 50 mm x 25 mm. In each case, at least two parallel-weighed specimens were exposed to the test solution with the help of a polytetrafluoroethylene (PTFE) specimen holder located at the bottom of a container. In each case, the volume of the solution was at the minimum of 5 ml/cm^2 based on the exposed area of the specimens [30]. The exposure time was 28 days. Following the tests, the specimens which were first rinsed with ion-exchanged water were weighed and subjected to characterization.

2.4. Characterization

The test materials were subjected to microstructural characterization before and after the corrosion experiments. The optical microscopy (OM) examinations in cross-section were conducted for as-received (etching solution for austenitic alloys: V2A, and for duplex grades: NaOH) materials using a Zeiss Axio Observer 7 optical microscope. The passive film compositions of the test materials prior to experiments were investigated by X-ray Photoelectron Spectroscopy (XPS) measurements using a ULVAC-Phi Quantum 2000 instrument. XPS investigations were conducted for wet-ground specimens that were then ultrasonically cleaned in acetone, rinsed with ethanol, dried, and let to oxidize for at least 18 h (treatment like for the specimens for electrochemical measurements). The spectra were obtained using a monochromatic Al Kα beam with a 100 μm spot size. In the case of duplex grades, such a spot size produced a combined data for the austenitic and ferritic phases. The elemental analyses were performed for O (O 1 s), Fe (Fe $2p_{3/2}$), Cr (Cr $2p_{3/2}$), Ni (Ni $2p_{3/2}$), Mo (Mo $3d_{5/2}$) and Mn (Mn $2p_{3/2}$). The analysis depth was in the range from 3 to 5 nm, enabled by the sputtering with Ar^+ with the acceleration voltage of 500 V. The measurements were followed by depth profiling for the same elements, at the sputtering rate of 1 nm min^{-1}.

After the experiments, the specimens were examined visually to detect the occurrence, form and extent of attack. The surfaces of specimens were further investigated by scanning electron microscopy (SEM), using a Zeiss ULTRAplus field emission (FE) SEM to define the corrosion form and investigate the details of the corrosion attack. Special emphasis was put on examining in detail the progress of pitting corrosion in the duplex grades of stainless steels in the immersion tests. For these studies, cross-sectional specimens and a FE-SEM Zeiss Crossbeam 540 equipped with an EDAX Hikari Plus electron backscatter diffraction (EBSD) detector and solid-state four-quadrant back-scattering electron (BSE) detector were used. EBSD analyses were conducted using the acceleration voltage of 20 kV at the working distance (WD) of 12–14 mm and the tilt angle of 70°. EBSD inverse pole figures (IPF) and phase mapping images were analysed using the TSL OIM Analysis 8 software. The BSE examinations were carried out at a smaller WD of 5–7 mm. Energy Dispersive X-Ray (EDX) analyses were conducted using an EDAX EDX detector attached to FE-SEM.

3. Results and discussion

3.1. Microstructural characterization

Optical microscopy studies of the test materials confirmed the duplex microstructure of grades 1.4662, 1.4462, and 1.4410, and the austenitic microstructure of grades 1.4539 and 1.4547, Fig. 1. In the duplex grades, the phase seen in the darker grey contrast was the ferrite phase, while the one seen in the lighter grey contrast was the austenite phase. The grains in the duplex grades of stainless steels were orientated the rolling direction of the material, and austenite phase existed as elongated islands within a relatively more continuous ferrite matrix. In the grade 1.4662, width of the austenite grains was approximately 20 μm, while in the grades 1.4462 and 1.4410 it was somewhat lower, in the range from 10 to 15 μm. The phase fractions and composition of the phases were estimated with ThermoCalc [31] software, Table 4. In austenitic grades, the crystals were larger and more equiaxed as compared to the duplex grades. The average grain size of the austenitic grades was approximately equal, ranging from 50 to 55 μm. XPS spectra were measured to define the composition and thickness of passive films on the investigated stainless steels, Fig. 2. Elemental depth profiles (Fig. 2a) indicated that chromium was enriched in the outer layer of the passive film, as the relative concentration of chromium in the vicinity of the surface was essentially higher than at greater depths. Cr depth profiles (Figs. 2b-F) disclosed that the thickness of the passive films varied between 1.0 nm (1.4410) and 1.75 nm (1.4462). In most cases (1.4529, 1.4662, 1.4547), the thickness was 1.5 nm.

3.2. Electrochemical experiments

Electrochemical experiments were performed to assess the electrochemical behaviour of the materials, in particular their susceptibility to pitting attack, and to guide the selection of test conditions for the immersion tests in the case of each material. Cyclic potentiodynamic polarization measurements (conducted after a period of open circuit potential monitoring) were chosen as the main method. Fig. 3 shows examples of cyclic potentiodynamic polarization curves for the five stainless steel grades in 1 wt.% H_2SO_4 in the absence and presence of NaCl (5000 mg/L) at 90°C. In 1%H_2SO_4 at 90 °C, all studied stainless steels exhibited a negative hysteresis, thus the probable corrosion attack would be general corrosion. However, 1% H_2SO_4 with 5000 mg/L NaCl at 90 °C, lower-PREN stainless steel grades 1.4662, 1.4539 and 1.4462 were susceptible to pitting attack, as indicated by the positive hysteresis loops in their cyclic potentiodynamic curves. However, in order to provide novel insights into the behaviour of the test materials in chloride-containing sulphuric acid solutions, the key electrochemical parameters derived from the curves, instead of the huge set of the original curves, are presented and analysed as a function of variables.

Thermodynamic and kinetic parameters describing corrosion behaviour of the test materials in 1 wt.% H_2SO_4 solution in the NaCl concentration range from 0 to 10,000 mg L^{-1} at the three test temperatures are shown in Figs. 4-7. The results from OCP measurements, Fig. 4a, revealed differences between the alloys but not so clearly between test temperatures or solution NaCl concentrations. The highest average OCP values were detected for the two austenitic alloys, 1.4539 and 1.4547, with the lowest OCP values being related to the duplex grades 1.4462 and 1.4410. The only systematic trend for all test materials with respect to temperature was that the lowest overall OCP values were detected at the temperature of 130°C. Otherwise, for some alloys (1.4662, 1.4547, 1.4410), the overall OCP values slightly decreased with an increase in temperature, but there were also materials (1.4539, 1.4462) for which an opposite trend was detected. No clear trend between OCP values and solution NaCl concentration was detected except for that in many cases, the lowest OCP values occurred at the middlemost NaCl concentrations.

Fig. 4b shows the correlation between the values of E_{corr} and OCP. The data points could be roughly divided into two categories. The main trend was the linear relationship between the values of E_{corr} and OCP; most of the values detected at the temperature of 130°C fell into this category, similarly to the data points representing the alloy 1.4539. In the case of the highest test temperature where the potential values belonged to the lower end of the potential scale, this likely reflects that

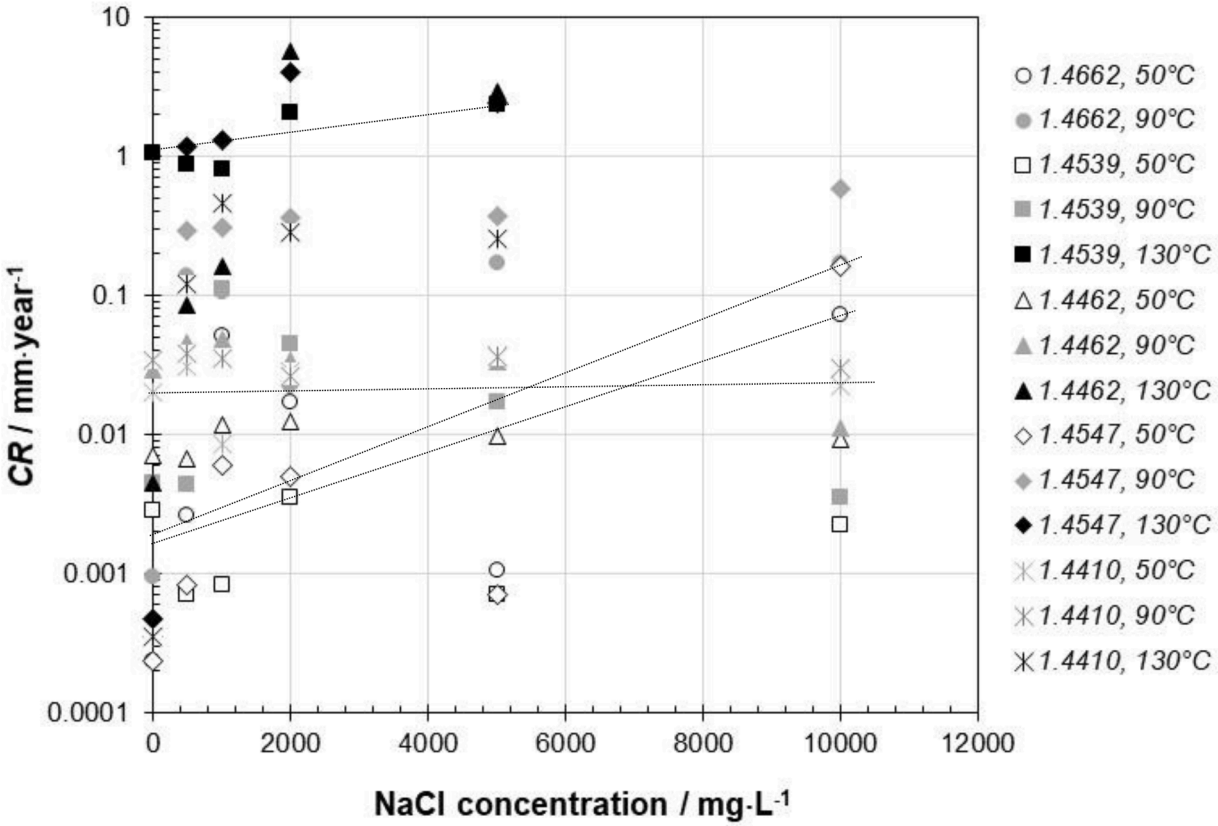

Fig. 5. Corrosion rate (CR) for the alloys in 1 wt.% sulphuric acid, defined based on the corrosion current density, i_{corr}. The presented lines are intended to guide the eye in some example cases.

the materials behaved in an equally active manner under both conditions, while the results for the grade 1.4539 at the high potential end of the axes suggest the opposite, i.e., consistent stability of the passive film. The second category of results cover the data points that are located below the linear trend line, i.e., for which the E_{corr} value was lower than OCP. This category embraced the majority of collected results: the data points representing the grades 1.4662, 1.4462, 1.4547 and 1.4410, and the temperatures up to 90°C. Their location may be explained by starting the polarization scans from the cathodic range, thus the air-formed passive layer likely spent some time under the conditions of lower oxidation capacity, leading to slightly lower E_{corr} values compared to OCP values, but essentially not to activation of the surface. Additionally, few random data points were situated above the linear trend line.

Although uniform corrosion was not in the focus of the research, the rate could be determined based on i_{corr} derived by extrapolating the electrochemical data. From the viewpoint of overall corrosion behaviour, it enables interesting comparisons between the materials and conditions, yet we acknowledge that the required first-order kinetics in the curves was not perfectly met in all cases, and that this approach may yield higher corrosion rates than obtained under equilibrium conditions. Fig. 5 summarizes the uniform corrosion rate (CR) values as a function of test variables. Indeed, the results revealed differences between the test temperatures and solution NaCl concentrations, and slightly between the stainless steel grades. In all cases, the corrosion rates for the materials increased with an increase in test temperature and NaCl concentration of the solution. The highest corrosion rates were systematically observed at the highest test temperature, reaching a level greater than 1 mm/a (high corrosion rate according to Outokumpu corrosion rate classification [19]). On average, the increase in the corrosion rate of the materials between the successive test temperatures (50, 90 and 130°C) was almost by one order of magnitude. The contribution of solution NaCl concentration to the corrosion rate of the materials was not as pronounced as that of test temperature, less than an order of magnitude in total. No evident trends between the CRs and stainless steel grades were detected.

Build-up and breakdown of passivity were investigated via key potential values: passivation potential, E_{pass}, breakdown potential, E_b, and repassivation potential, E_{rep}, Fig. 6. Examination of the values for E_{pass} revealed differences between the five stainless steel grades and some of the test conditions. amongst the test materials, the highest values for E_{pass} were detected for the two austenitic grades: 1.4547 and 1.4539. In contrast, by far the lowest overall values for E_{pass} were measured for the duplex grade 1.4410. As for the influence of the environmental characteristics on the values for E_{pass}, the main observation was that the highest test temperature, 130°C, typically introduced the lowest E_{pass} values; this was true for all test materials except for the grade 1.4410. Further insights into the passive film build-up were obtained via examining the difference between passivation and corrosion potentials, E_{pass}-E_{corr}, following ref. [20] (Fig. 6b). This approach disclosed the highest E_{pass}-E_{corr} values for the grades 1.4547 and 1.4662, whereas the lowest E_{pass}-E_{corr} values were related to the grade 1.4410. These results may be interpreted so that the build-up of the passive film on grades 1.4547 and 1.4662 requires relatively greater deviation from the equilibrium compared with the other alloys, and that the passivation of grade 1.4410 occurs with ease. No clear trend between the test temperatures or solution NaCl concentrations and the values for E_{pass}-E_{corr} could be detected. The analysis of E_b values showed the dependence of the parameter on temperature, NaCl concentration, and alloy composition (Fig. 6c). At the lowest test temperature, 50°C, E_b values for all five grades of stainless steel fell in the range from 810 to 920 mV vs. Ag/AgCl

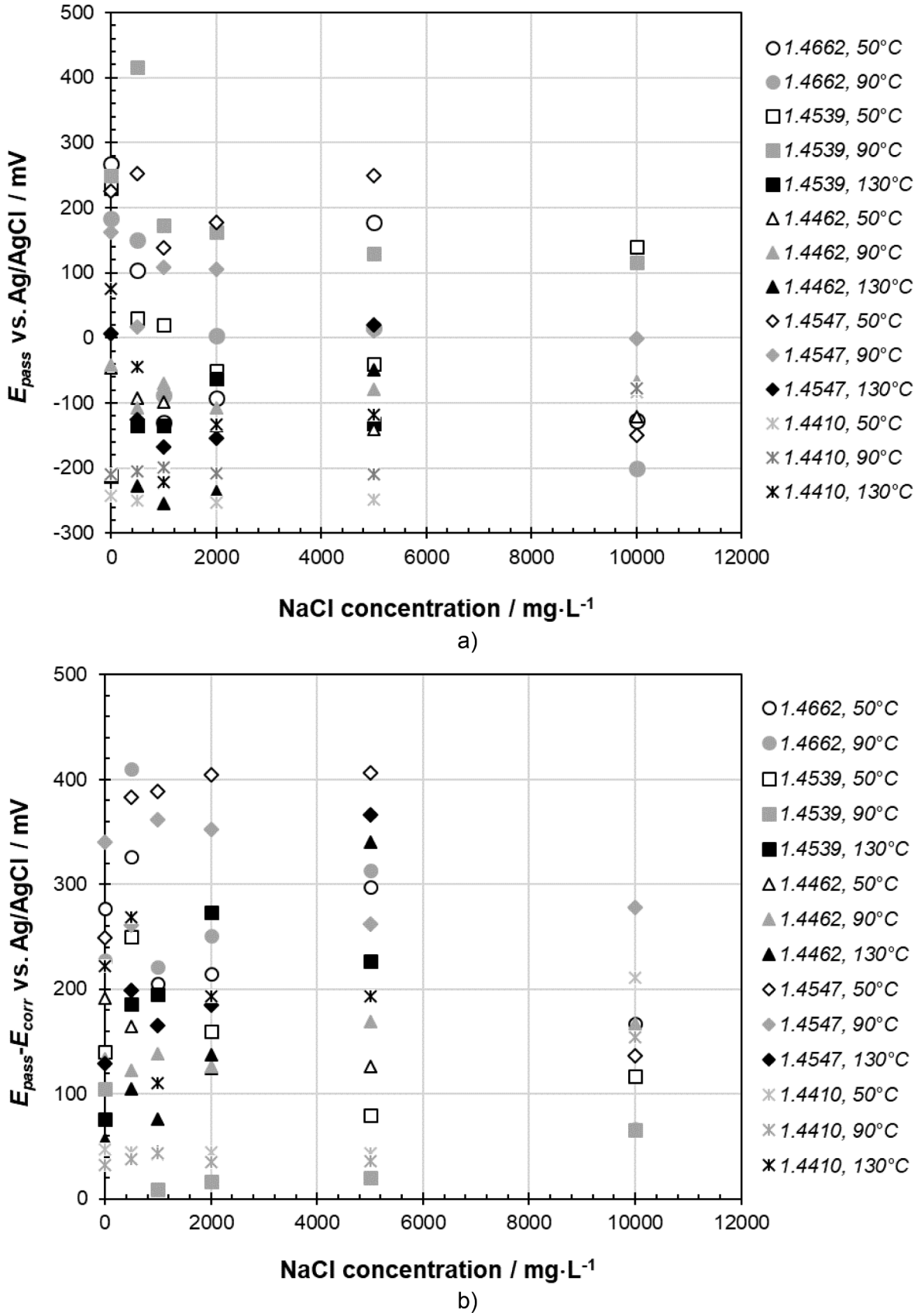

Fig. 6. Important potential values for the passivity of the alloys in 1 wt.% sulphuric acid. a) Passivation potential, E_{pass}. b) E_{pass}-E_{corr}. c) Breakdown potential, E_b. d) E_b as a function of chloride activity, a_{Cl^-}. e) Repassivation potential, E_{repass}. In d), the presented lines are intended to guide the eye in some example cases.

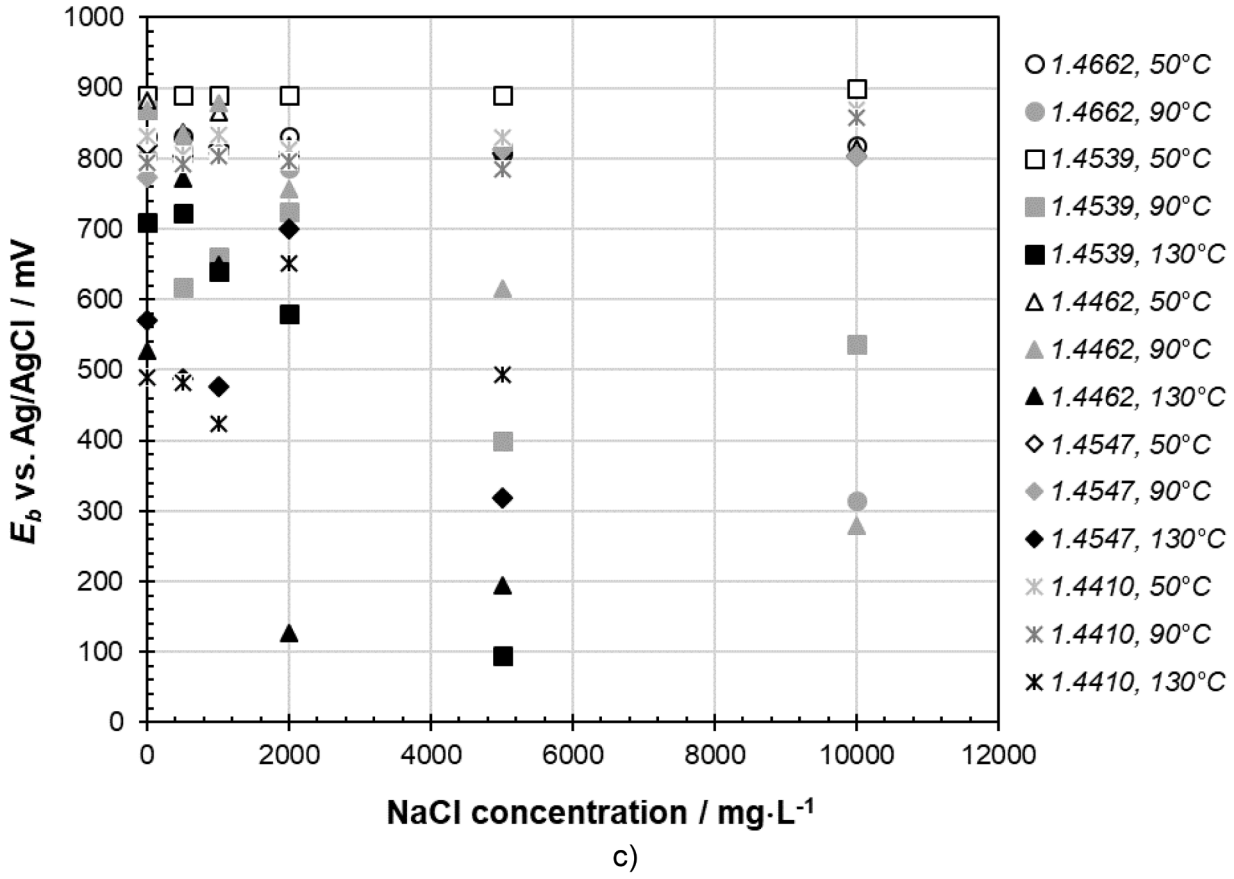

c)

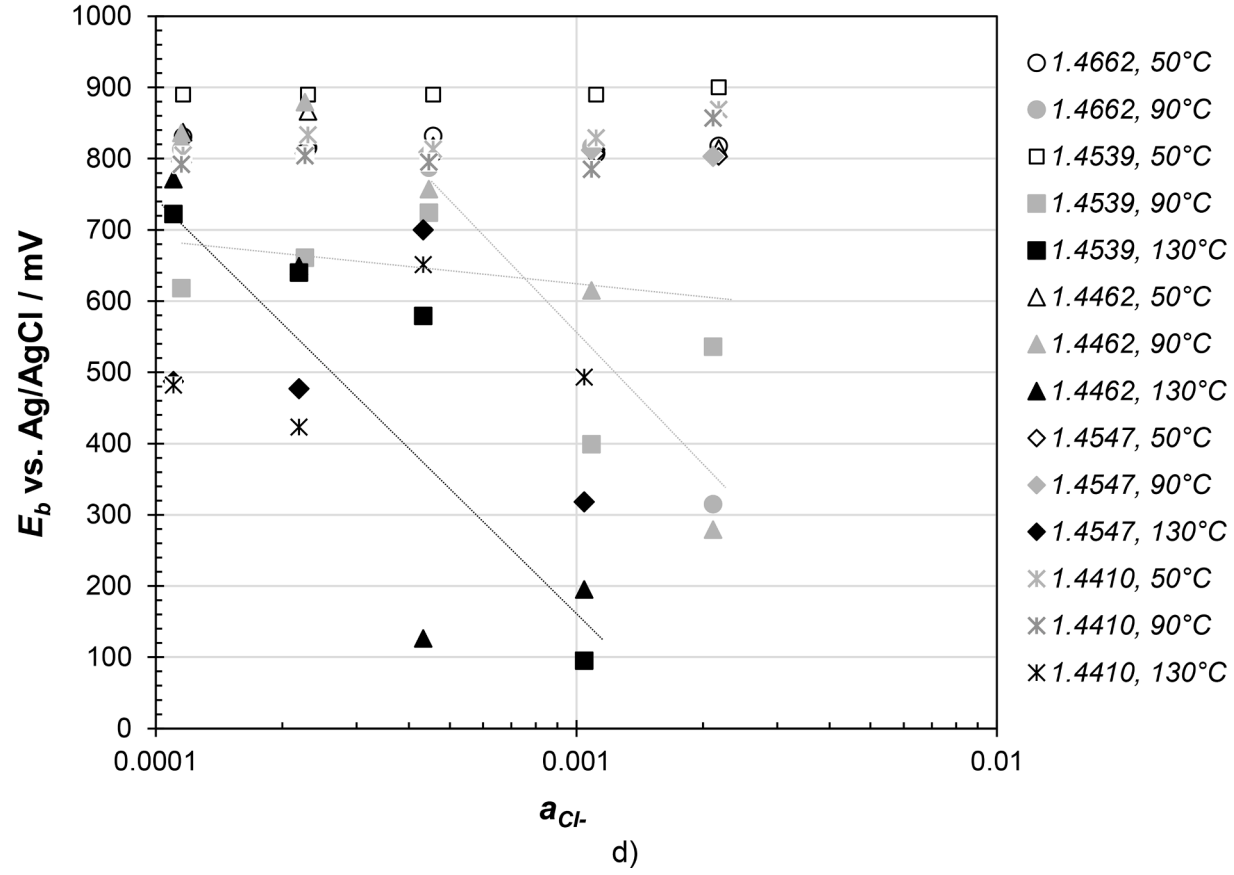

d)

Fig. 6. (*continued*).

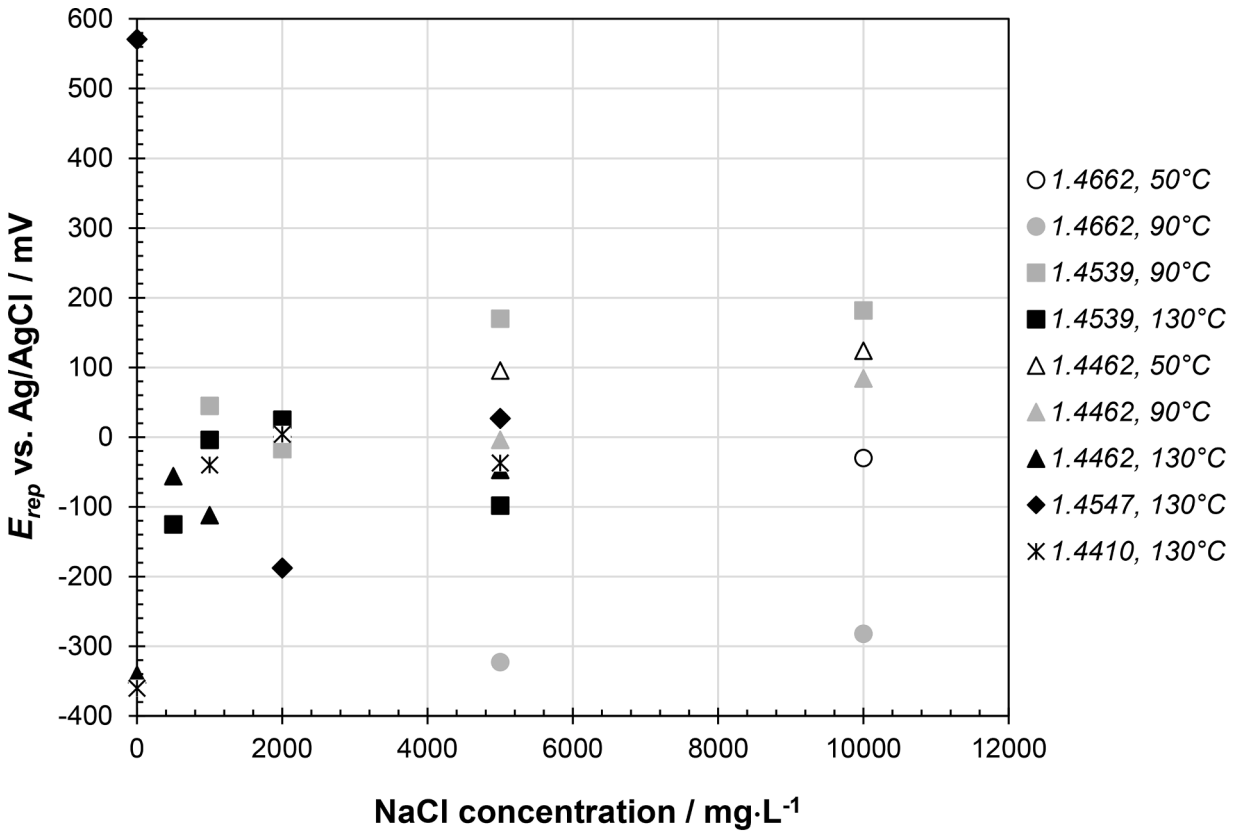

e)

Fig. 6. (*continued*).

irrespective of solution NaCl concentration, corresponding to transpassivity rather than passivity breakdown. However, E_b values decreased with an increase in temperature. At the temperature of 90°C, particularly at the highest NaCl concentrations, E_b values for some of the test materials were clearly lowered from the transpassivity range, hence passivity breakdown occurred. Such situations occurred for the three alloys with PREN in the range from 33 to 35: for the grade 1.4662 at the NaCl concentration of 10,000 mg/L, for the grade 1.4539 over the NaCl concentration range from 500 to 100,000 mg/L and for the grade 1.4462 at NaCl concentrations 2000, 5000 and 10,000 mg/L. For the two alloys with higher PREN (1.4547 and 1.4410), E_b values at 90°C fell within the transpassivity potential area. At the highest test temperature, E_b values for all studied materials and NaCl concentrations were much lower than the transpassivity range, suggesting passivity breakdown in all cases. The values for E_b decreased with an increase in both temperature and solution NaCl concentration. A detailed analysis of E_b as a function of solution chloride activity, a_{Cl^-}, Fig. 6d, revealed some linearity between E_b and a_{Cl^-} values in many cases, where passivity breakdown occurred. The examination of values for E_{rep} (Fig. 6e) disclosed mainly a decreasing trend with increase in temperature.

As defined by McCafferty [32], active-passive transition occurs at a so-called Flade potential, at which the current density values related to active dissolution are at maximum and start to decrease with increase in potential. The current density at the Flade potential is called critical current density for passivation, i_{crit}, because it indicates the extent of anodic dissolution that is needed to reach the passivity. Therefore, i_{crit}, is a parameter that reflects the ease of passivation in such cases where a clear shift from active to passive state occurs and, if there is no clear i_{crit}, the passivation is spontaneous [33]. It has been shown [32] that i_{crit} typically increases with increase in solution pH, implying that greater extent of preceding anodic dissolution is necessary towards more acidic solutions. Insights into the values of i_{crit}, Fig. 7a, revealed differences between the alloys and temperatures. First of all, grade 1.4539 did not exhibit a clear i_{crit} in all polarization curves at the two lowest test temperatures, thus the passivation was easy and did not require a notable contribution by the preceding anodic dissolution. amongst the other alloys, the lowest i_{crit} values were observed for the grades 1.4547 and 1.4662, while the highest overall i_{crit} values were associated with the grade 1.4462, suggesting that the passivation of this alloy required a significant preceding anodic dissolution. As can be seen in Fig. 7a, the values of i_{crit} increased with an increase in temperature, reflecting that passivation of surfaces became more difficult. At the lowest temperature, the values of i_{crit} were low, at the maximum of the magnitude of typical current density values in the passive region, 1–2 μA/cm^2. With the increase in temperature to 90°C, the average values of i_{crit} were of the magnitude of 7 μA/cm^2, while further temperature rise to 130°C shifted the average values of i_{crit} by several orders or magnitude, up to 0.5 mA/cm^2. A slight increasing trend between the solution NaCl concentration and the values of i_{crit} could be detected, particularly at the two highest test temperatures. The passive current density i_{pass} for the alloys, Fig. 7b, is proportional to the dissolution rate of the material in the passive region. At the lowest temperature, the values of i_{pass} were below 1 μA/cm^2 for all alloys except for 1.4539 and 1.4462. With increase in temperature to 90°C, the average i_{pass} values for alloys with PREN of 33–35 (1.4662, 1.4539, 1.4462) increased to the level 2–4 μA/cm^2, while those for the higher PREN alloys (1.4547, 1.4410) were retained

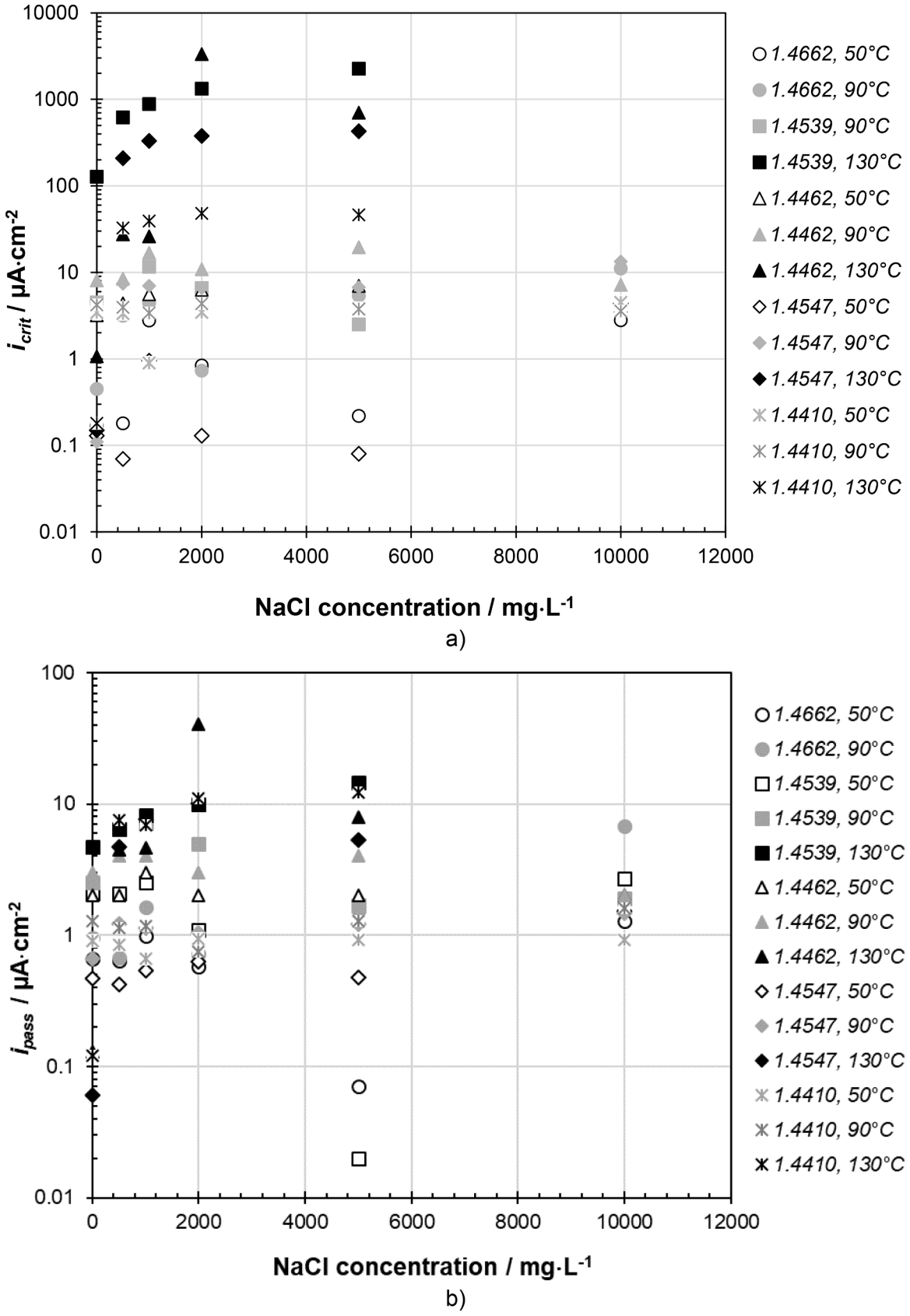

Fig. 7. Current density values important for passivation for the three grades of stainless steel in 1 wt.% H_2SO_4. a) Critical current density for passivation, i_{crit}. b) Passive current density, i_{pass}.

Table 5
Summary of overall corrosion behaviour of the alloys (PRENs in brackets). *P* indicates pitting corrosion. The rate of uniform corrosion is presented in colours as follows: *green* corrosion rate <0.1 mm/a, *yellow* corrosion rate in the range 0.1–1.0 mm/a, *red* corrosion rate >1.0 mm/a. Grey: experiments were not conducted.

Temperature, °C	NaCl concentration, mg L^{-1}	$a(Cl^-)/a(SO_4^{2-})$	1.4662 (33.4)	1.4539 (34.3)	1.4462 (35.4)	1.4547 (42.8)	1.4410 (43.8)
50	0	0					
	500	1.7					
	1000	3.3					
	2000	6.7					
	5000	16.8					
	10,000	34.2					
90	0	0					
	500	5.3		*P*			
	1000	10.3		*P*			
	2000	20.5		*P*	*P*		
	5000	50.3		*P*	*P*		
	10,000	99.4	*P*	*P*	*P*		
130	0	0			*P*	*P*	*P*
	500	19.1		*P*	*P*	*P*	*P*
	1000	38.0		*P*	*P*	*P*	*P*
	2000	74.9		*P*	*P*	*P*	*P*
	5000	181.3		*P*	*P*	*P*	*P*

at the same level than at the lower temperatures. At the highest temperature, the i_{pass} values for all materials were several μA/cm^2, thus clearly higher than at lower temperatures, indicating the dissolution of the passive film, i.e., uniform corrosion. amongst the test materials, the highest overall i_{pass} values were detected for grade 1.4462.

Table 5 summarizes the key results from the electrochemical measurements as a function of test conditions. The differences in corrosion behaviour between the alloys became evident at the temperature of 90°C. Based on the results, grade 1.4539 was susceptible to pitting attack in the widest NaCl concentration range at 90°C, from 500 mg/L upwards, followed by the duplex grades 1.4462 (≥2000 mg/L) and 1.4662 (10,000 mg/L). At the highest test temperature, pitting corrosion was detected in all test materials, yet dissolution of the passive film introduced parallel uniform corrosion of the alloys, as indicated by the high i_{pass} values. amongst the studied five alloys, the resistance to both forms of attack: pitting corrosion and uniform corrosion, was the best in the case of 1.4410, i.e., the alloy with the highest PREN and Cr content. It is worth mentioning that conversely to what we have earlier reported for the alloys with the PREN of 25–26 [20], we could not detect any correlation between the solution chloride to sulphate activity ratio, $a(Cl^-)/a(SO_4^{2-})$, and materials' susceptibility to pitting corrosion. This likely correlates with the greater resistance of the passive layer against the passivity breakdown in the alloys included in this work (PRENs in the range from 33 to 44) compared to those in ref. [20], making the phenomena, such as the adsorption of inhibitive species, less meaningful than in such cases where passivity breakdown is easier.

3.3. Immersion tests

In order to have a better understanding of the corrosion behaviour of the materials, immersion experiments of the duration of 28 days were conducted at the temperature of 90°C. Table 3 shows the combination of materials and electrolyte compositions included in immersion tests. The test matrix targeted particularly such NaCl concentrations below which we did not detect pitting corrosion for each of the materials in electrochemical measurements, but above which pitting corrosion was observed (Table 5). Electrochemical methods: OCP measurements and redox potential measurements were used to provide supportive mechanistic information about the materials behaviour.

The results from OCP measurements for the five test materials in each test solution during the first 24 h of the immersion test are shown in Fig. 8, enabling several general findings to be made. First, the lowest OCP values for materials amongst the test solutions were typically recorded in solutions containing only sulphuric acid and NaCl (electrolytes #1–4), implying that the presence of metallic cations (Fe^{3+}, Fe^{2+}, Cu^{2+}) raised the OCP level, as predicted. Second, the highest OCP values for all five test materials were detected in electrolytes that contained ferric ions, Fe^{3+}. Additionally, the highest OCP values for the materials were often detected in such cases where the Fe^{3+} content was higher, 5000 mg/L, although this was not the case in all studied systems (e.g., grade 1.4662 #12). Third, the OCP values for the alloys were consistently higher in electrolytes with ferric ions, Fe^{3+}, as compared to the environments with an equal concentration of ferrous ions, Fe^{2+}, or cupric ions, Cu^{2+}. This can be seen particularly in the immersion tests conducted for the grades 1.4462 (#8 vs. #11, #8 vs. #10, Fig. 8c) and 1.4410 (#13 vs. #16, #13 vs. #15, #19 vs. #21, Fig. 8e). Fourth, further addition of sulphate ions, SO_4^{2-}, into the metal cation containing test environments altered the OCP of the material slightly, by approximately 100 mV, typically by lowering it (alloy 1.4539 #8 vs. #9, alloy 1.4462 #11 vs. #17, alloy 1.4410 #19 vs. #20). However, also an increase by an equal extent was detected (alloy 1.4539 #13 vs. #14). Fifth, solely NaCl concentration of the solution did not determine the OCP levels detected for the materials in the electrolytes. For example, in the case of alloy 1.4462, the OCP values amongst the H_2SO_4–NaCl solutions (#2, #3 and #4) were lowest in the solution containing the highest amount of NaCl, #4. However, the opposite trend was observed for the alloy 1.4410 in the H_2SO_4–NaCl solutions #3 and #4, with clearly the lower OCP levels being detected in 2000 mg/L NaCl containing solution #3 than in the 5000 mg/L NaCl bearing solution #4. In solutions containing metallic cations, the highest OCP levels for alloys 1.4662, 1.4539 and 1.4462 were detected in Fe^{3+} containing solutions with 1000 mg/L or 2000 mg/L NaCl although the experiments were also conducted using higher NaCl concentrations, whereas for the grade 1.4410, the highest OCP level was detected in Fe^{3+} bearing solution with the highest NaCl content. Additionally, the OCP levels for each test material varied significantly and about equal potential values between the electrolytes with different compositions; thus, the material composition did not directly correlate with the detected OCP levels.

Weight loss in the specimens during the immersion tests is shown in Fig. 9. amongst the test materials, the highest material losses were detected in the case of specimens of grade 1.4662, while the lowest overall material losses occurred in the specimens of grade 1.4410. Indeed, in the case of grade 1.4662 (Fig. 9a), weight losses with the extent of as high as 1.4 and 1.3 mg/(cm^2·d) were detected in electrolytes that contained 5000 mg/L Fe^{3+}, #19 (5000 mg/L NaCl) and #13 (2000 mg/L NaCl). In the corresponding electrolytes with lower Fe^{3+} concentration, 500 mg/L, the weight losses for the specimens of grade 1.4662 were 0.3 mg/(cm^2·d) (#18) and 0.2 mg/(cm^2·d) (#12), whereas

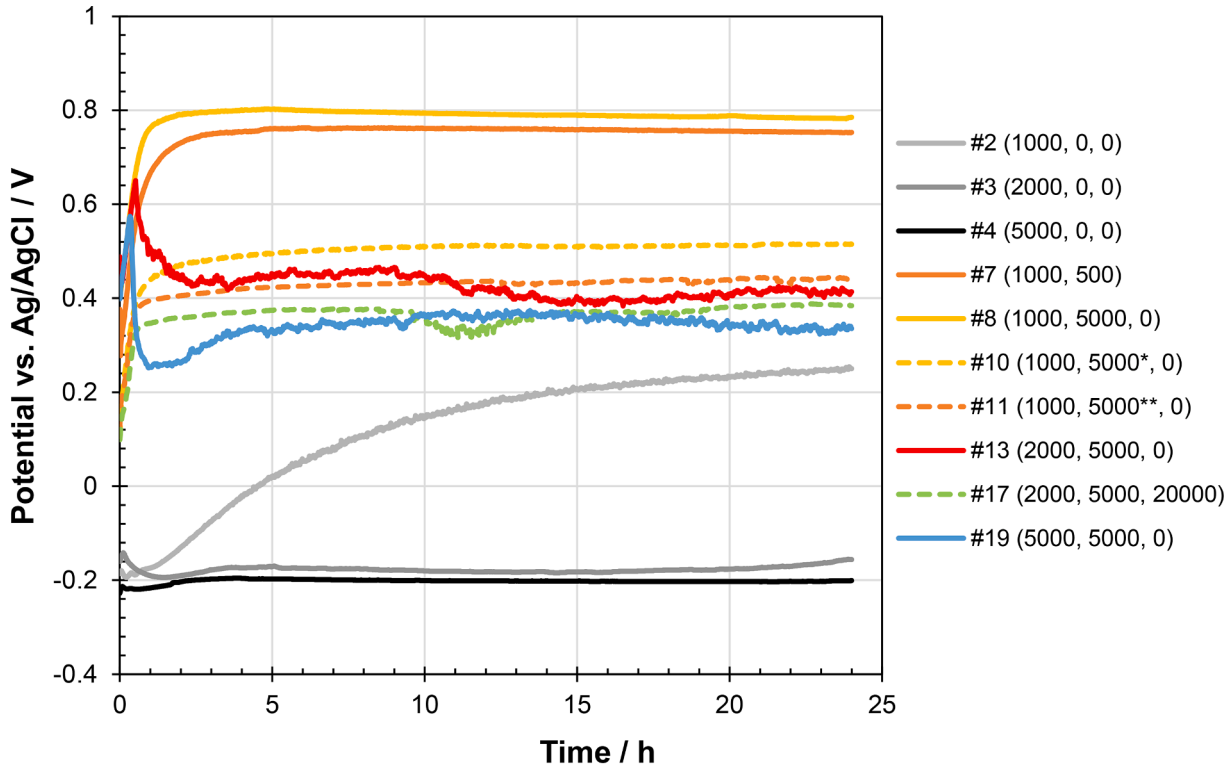

c)

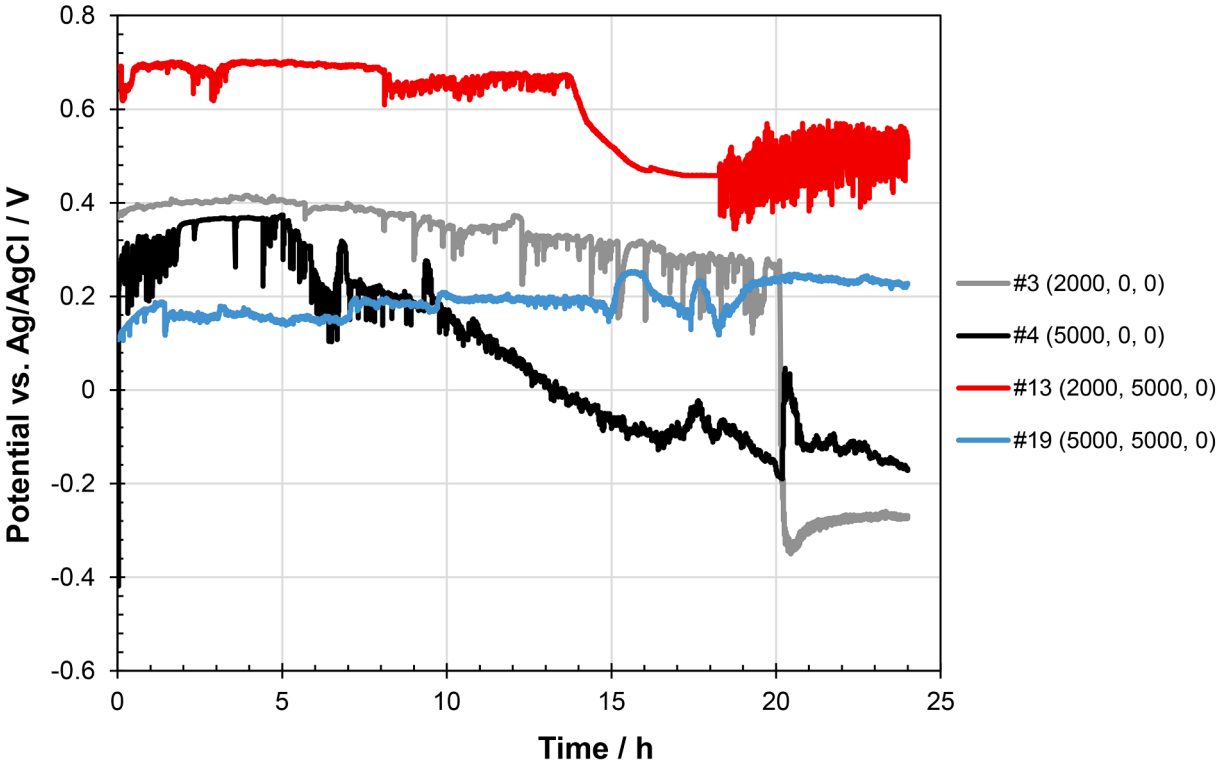

d)

Fig. 8. Open circuit potential records for a) 1.4662, b) 1.4539, c) 1.4462, d) 1.4547 , e) 1.4410. The values in parentheses represent the concentrations of following species: NaCl, Fe^{3+} and SO_4^{2-} in mg/L. amongst the values for Fe^{3+}, * indicates that the used metal cations were Cu^{2+}, while ** indicates that the used metal cations were Fe^{2+} (instead of Fe^{3+}).

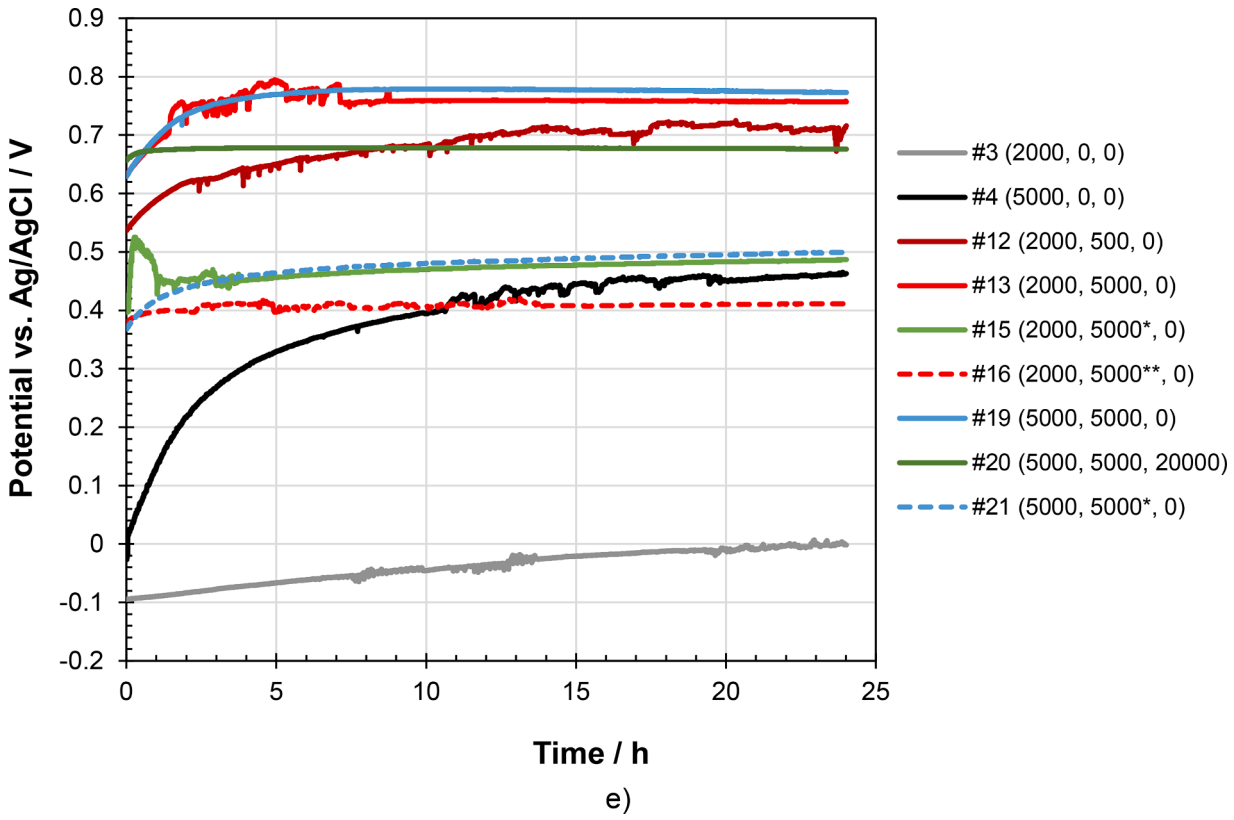

Fig. 8. (*continued*).

in all other electrolytes the specimen weight changes were negligible. As for grade 1.4539 (Fig. 9b), weight losses were detected in most of the studied electrolytes. The highest weight losses for 1.4539 occurred in H_2SO_4–NaCl "base electrolytes" #1 and #2 with 500 mg/L and 1000 mg/L NaCl, amounting 0.5 and 0.4 mg/(cm^2·d), respectively, and in electrolyte #13 with 5000 mg/L Fe^{3+} and 2000 mg/L NaCl, 0.4 mg/(cm^2·d). Additionally, weight losses with the extent of 0.2 mg/(cm^2·d) or lower were detected in Fe^{3+} containing electrolytes #5, #7, #8 and #14. In the case of grade 1.4462 (Fig. 9c), greatest weight losses of 0.7 and 0.6 mg/(cm^2·d) were detected in electrolytes #19 and #13 with 5000 mg/L Fe^{3+} besides 5000 and 2000 mg/L NaCl, respectively. Additionally, minor weight losses of 0.1 mg/(cm^2·d) were detected in specimens exposed to #7 with 500 mg/L Fe^{3+} and 1000 mg/L NaCl. In the case of higher-PREN grades 1.4547 (Fig. 9d) and 1.4410 (Fig. 9e), significant weight losses occurred only in one electrolyte, namely #19 with 5000 mg/L NaCl and 5000 mg/L Fe^{3+}, in both cases.

Based on the above, it is evident that the presence of ferric ions, Fe^{3+}, is often linked with significant weight losses, particularly in 5000 mg/L NaCl containing electrolytes #19 (5000 mg/L Fe^{3+}) and #13 (500 mg/L Fe^{3+}). Indeed, the influence of ferric ions, Fe^{3+}, on the system electrochemistry is presented in Fig. 10. Already minor additions of ferric ions, 500 mg/L or even less, increased the redox potential of the solution from the value of approximately 600 mV vs Pt to the level of 800 mV vs Pt. Further ferric ion additions did not significantly change the redox potential of the electrolyte, i.e., the redox potential stabilized at about 800 mV vs Pt. The observation can be explained by the standard electrode potential values of the redox pair Fe^{3+}/Fe^{2+}: 0.770 V [34]. The standard electrode potentials of other potential redox systems: Fe^{3+}/Fe: −0.037 V, Fe^{2+}/Fe: −0.447 V and Cu^{2+}/Cu 0.342 V, also account for the relatively more important role of ferric ions as compared to ferrous ions, Fe^{2+}, or cupric ions, Cu^{2+}. A parallel trend to the electrolyte redox was observed in OCP of the test materials: an initial increase followed by a plateau. In the case of duplex grades 1.4662 and 1.4462, the plateau occurred at 350–400 mV vs. Ag/AgCl, while it was slightly lower for austenitic grade 1.4539, 200 mV vs. Ag/AgCl. In the case of higher-PREN alloys 1.4547 and 1.4410, the plateau was located at about 750 mV vs. AgCl. Comparing these values to Figs. 6c-d discloses that the OCP plateau for grades 1.4662 and 1.4462 was at a higher level than the breakdown potentials of the materials, suggesting that ferric ions easily give rise to passivity breakdown. The opposite trend was detected for the test materials 1.4539, 1.4547 and 1.4410: their E_b values were higher than the OCP plateau by ferric ions.

Consistent with the electrochemistry results, differences were evident between the five stainless steel grades with respect to the form of attack. In the case of austenitic alloys 1.4539 and 1.4547, in the absence of additional metal cations Fe^{3+}, Fe^{2+} and Cu^{2+} (Fig. 11a-d), corrosion in the surfaces progressed primarily as uniform corrosion. In such cases, the alloy surfaces after the tests were matt in appearance, in contrast to the original shine. In the presence of oxidizing cations, particularly ferric cations Fe^{3+}, the attack in austenitic grades progressed as localized corrosion of the edges (Fig. 11e-i), while the large surfaces were retained shiny and unaltered.

In the case of duplex grades 1.4662 and 1.4462, pitting corrosion was clearly the dominant form of attack (Figs. 12-15). The surfaces of grade 1.4662 typically contained few large pits, in which the attack followed the grain structure (Fig. 12a-d); the large pit size explains the highest weight losses amongst the immersion test specimens and likely reflects the relative ease of pit grown as compared to pit initiation. More detailed EBSD analyses revealed that the attack advanced essentially along the ferrite phase (BCC crystal structure) seen in green colour in the phase contrast map and located as narrow ribbons between the sections of austenite, Fig. 12e and f. This is consistent with the lower PREN of the ferrite phase as compared to that in the austenite phase in the alloy, Table 4. Earlier, Garfias-Mesias et al. [28] and Guo et al. [35] have reported the preferential pitting attack of the ferrite phase in 25Cr duplex stainless steel when exposed to chloride solutions. Additionally, Tsai and Chen [36] have demonstrated in H_2SO_4–HCl mixtures that the ferrite phase included in the grade 1.4462 was anodic compared to the

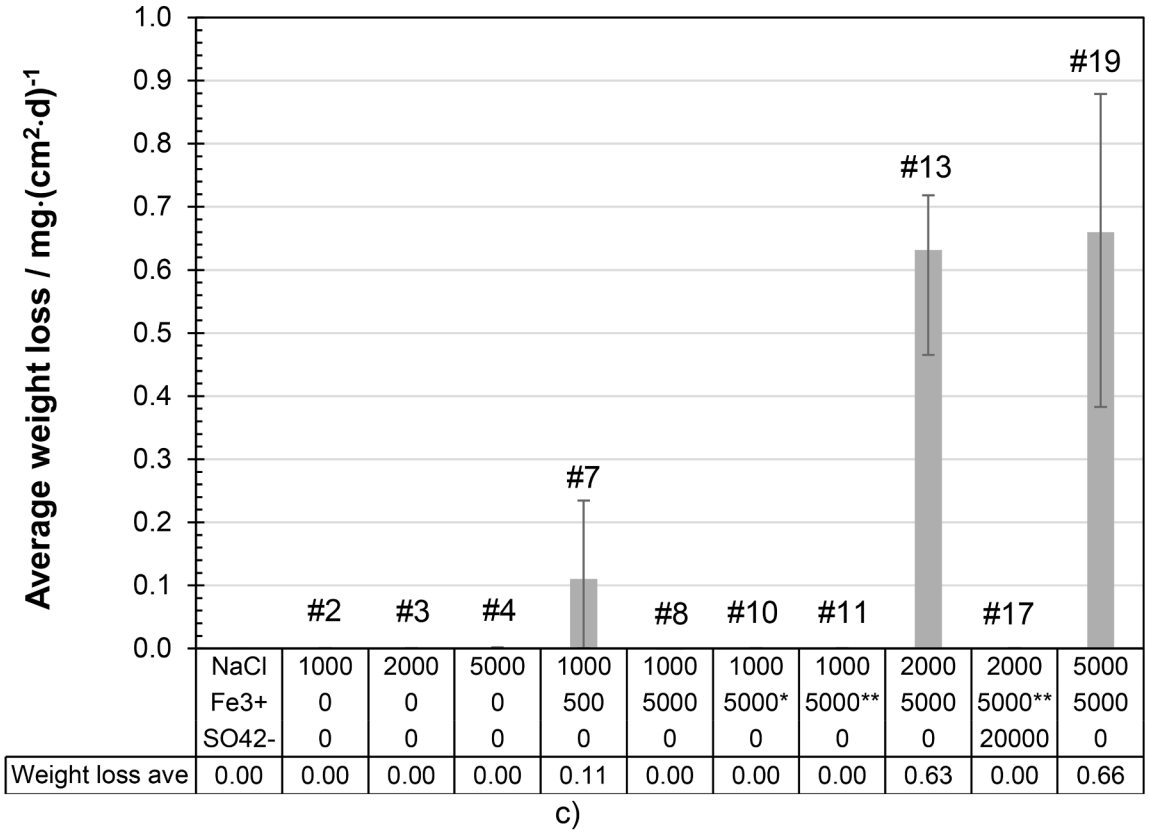

NaCl	1000	2000	5000	1000	1000	1000	1000	2000	2000	5000
Fe3+	0	0	0	500	5000	5000*	5000**	5000	5000**	5000
SO42-	0	0	0	0	0	0	0	0	20000	0
Weight loss ave	0.00	0.00	0.00	0.00	0.11	0.00	0.00	0.00	0.63	0.00	0.66

c)

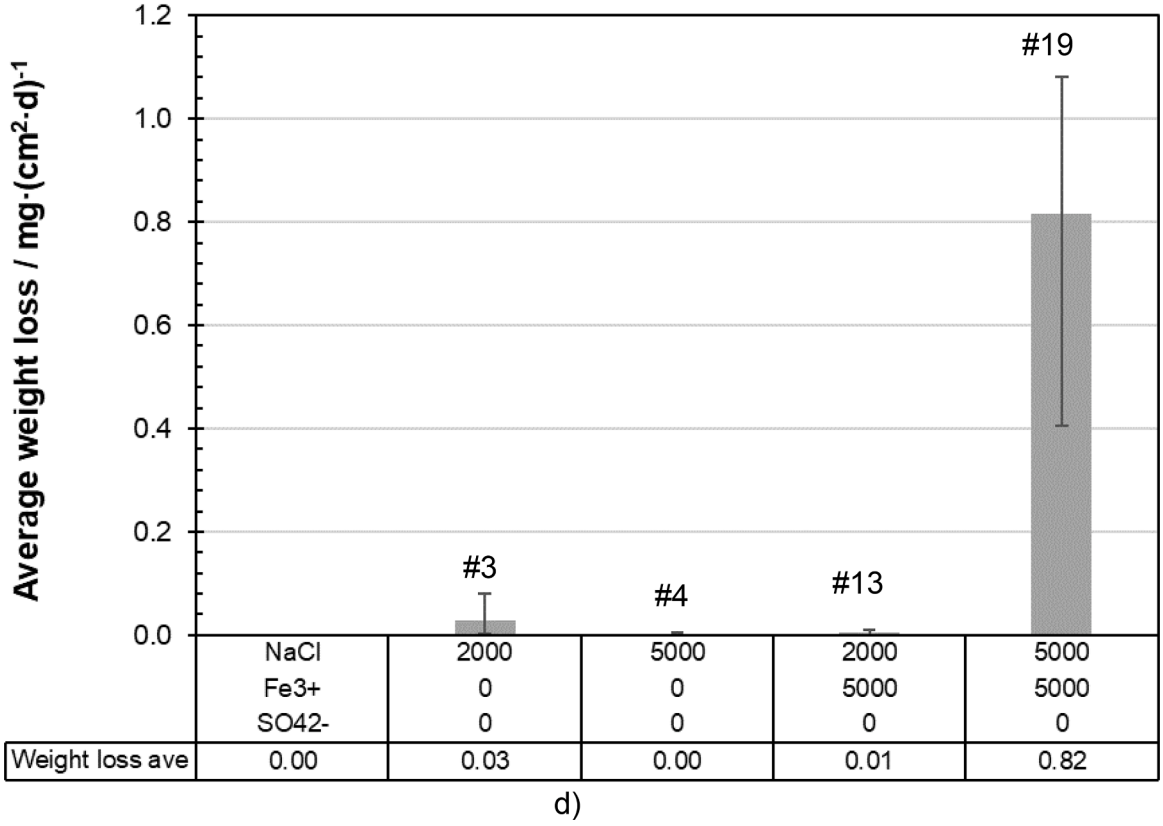

NaCl	2000	5000	2000	5000
Fe3+	0	0	5000	5000
SO42-	0	0	0	0
Weight loss ave	0.00	0.03	0.00	0.01	0.82

d)

Fig. 9. Average weight loss for the specimens during the immersion tests. a) 1.4662, b) 1.4539, c) 1.4462, d) 1.4547, e) 1.4410. In the tables, * indicates that the used metal cations were Cu^{2+}, while ** indicates that the used metal cations were Fe^{2+} (instead of Fe^{3+}).

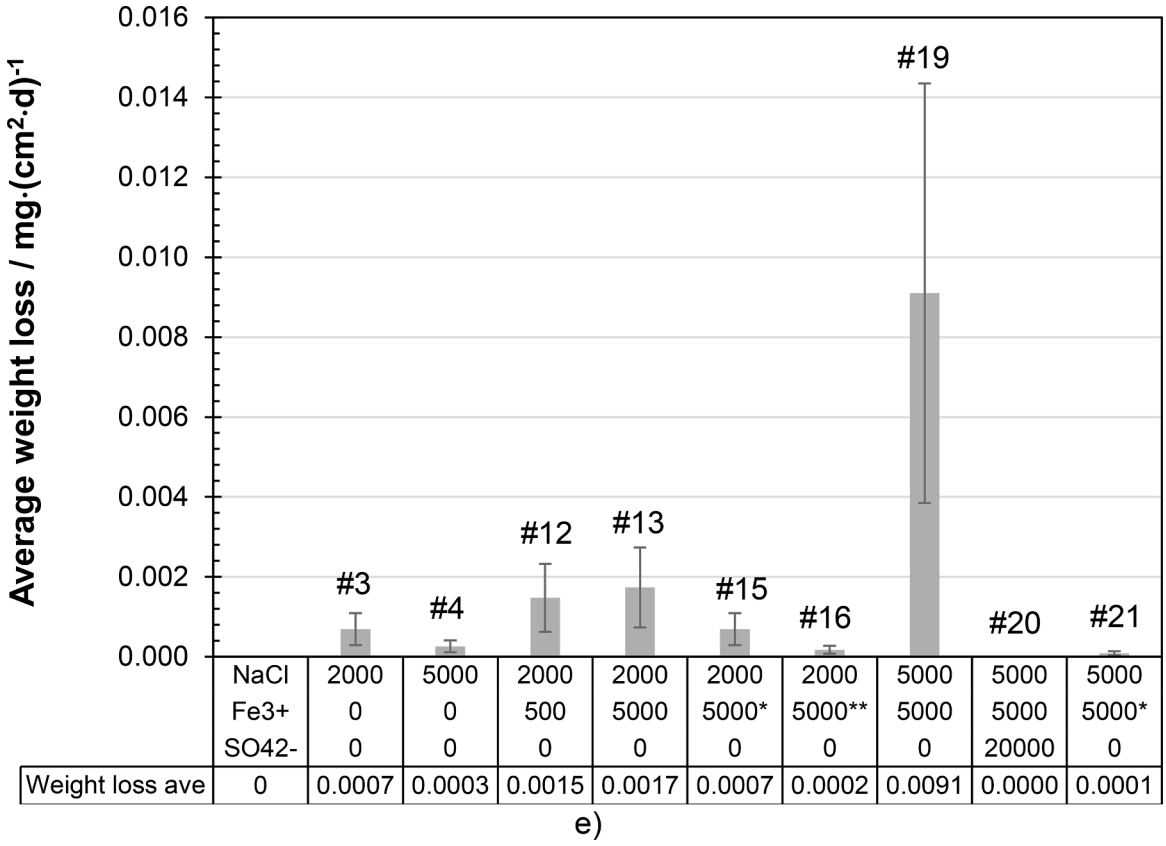

Fig. 9. (*continued*).

austenite phase, yet changing the electrolyte to HNO_3 reversed the polarity between the phases. EDS maps, Fig. 13, revealed that the ferrite phase was relatively enriched in chromium and molybdenum, while the austenite phase contained relatively more nickel and nitrogen, consistent with the literature [3,28,35] and the computational data (Table 4). The differences in the contents of the main alloying elements (Cr, Mo, Ni) between the phases were typically of the order of 2–3%, the magnitude of which is consistent with earlier compositional comparisons between the two phases [28,35], and quite well in agreement with the computed phase compositions (Table 4). Nevertheless, we emphasize that the exact composition of the phases was difficult to define, due to thin sections of alternating phases in the microstructure and the fact that the EDS signal also originates from the areas below the surface. In the specimens of duplex grade 1.4462, the surfaces were occasionally covered by a colourful, mostly violet, oxide film that underwent spalling and cracking (Fig. 14a) and contained numerous small pits (Fig. 14b-d). EBSD investigations (Fig. 14e and f) showed that, within the duplex microstructure, attack occurred preferentially along the austenite phase, consistent what has been reported earlier by, e.g., Deng et al. [37]. Again, this is consistent with the relatively lower PREN of the austenite phase as compared to that of the ferrite phase in the alloy, Table 4. For this stainless steel grade, elemental mapping disclosed differences between the Cr, Mo and Ni contents of the phases but not significantly between the N contents (Fig. 15). The finding is supported by the computed phase composition data (Table 4). Similarly to the grade EN1.4662, Cr and Mo were enriched in the ferrite phase, while Ni was concentrated in the austenite phase.

The results from electrochemical measurements and immersion experiments proved that the two duplex grades with PRENs in the range from 33 to 35, i.e., 1.4662 and 1.4462, were susceptible to pitting corrosion in the dilute sulphuric acid with NaCl. The relative compositions of the austenitic and ferritic phases, which to their PREN values, determine the preferential attack paths in the material. Our findings demonstrated that it was systematically the phase with the lower PREN value where the passivity breakdown occurred in the first place. It is known that nitrogen alloying has a radical influence on PREN by the multiplier of 16 (as compared to 1 of chromium and 3.3 of molybdenum, Eq. (1)) [21]; therefore the differences in nitrogen content between the two alloys and especially between the included ferrite and austenite phases easily explain the observations. Indeed, in the alloy with higher nitrogen content and clear differences in nitrogen alloying between the phases, i.e., the grade 1.4662, pitting attack preferentially occurred in the ferrite phase which is essentially deficient in nitrogen as compared to the austenite phase. Conversely, in the case of alloy 1.4462, where the overall nitrogen alloying level was lower and the relative differences in nitrogen alloying between the phases were lower, the austenite phase was the preferential attack site. In the case of austenitic stainless steel grade 1.4539 with the PREN of 34, the results from electrochemical measurements (Table 5) indicated pitting corrosion, yet uniform corrosion was the primary type of attack in immersion tests. As compared to the duplex grades 1.4662 and 1.4462, the absence of pitting corrosion in the austenitic grade 1.4539 may be explained by a slightly higher PREN of the alloy as compared to the lower-PREN phase in the duplex grades (1.4662: 33.1, 1.4462: 33.5). The absence of pitting corrosion in the grades 1.4547 and 1.4410 may be explained by their higher PREN values.

In literature, the beneficial effects of nitrogen alloying on the corrosion behaviour of stainless steels have been associated with, e.g., the increase in breakdown potential E_b [38,39] and better tendency to repassivation [28]. In this work, we could not directly correlate the presence of specific alloying elements, such as nitrogen, with the any individual electrochemical parameter, as the work covered five alloys with varying concentrations of several alloying elements. Instead, we did the analysis based on the PREN, which covers the joint contribution

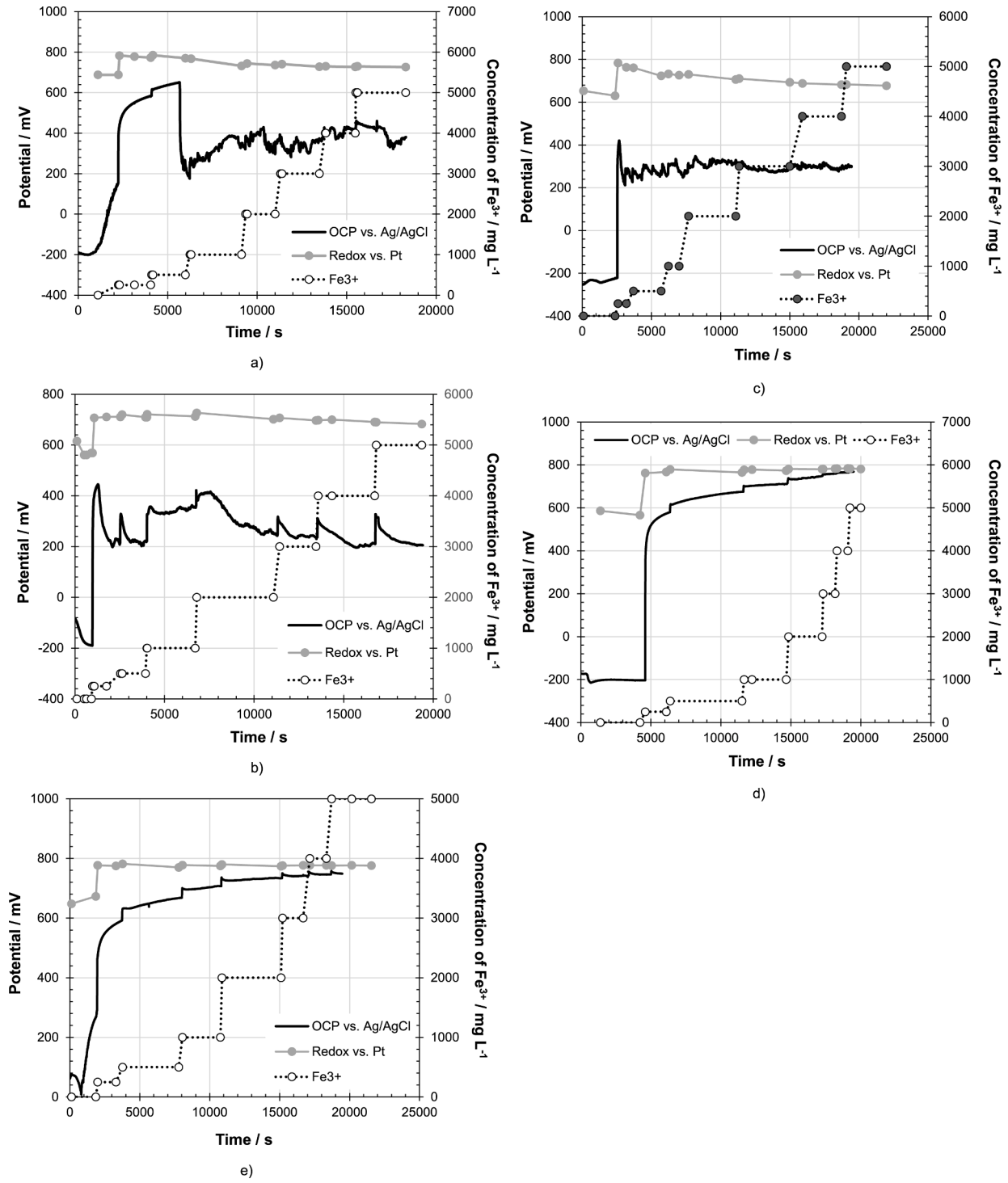

Fig. 10. Correlation between OCP of the studied stainless steels, redox of the solution and concentration of Fe^{3+} upon controlled Fe^{3+} additions. a) 1.4662. b) 1.4539. c) 1.4462. d) 1.4547. e) 1.4410. NaCl content of the solution was 5000 mg/L, while the test temperature was 90°C.

by all the key alloying elements. However, what is special in duplex grades is that the composition influences not only the PREN but also the partitioning of the alloying elements between the two phases and the overall phase fractions [3,28,40,41]. This is because nitrogen alloying modifies the phase diagram by expanding the austenite stability area [3] and the two phases (ferrite with BCC structure and austenite with FCC structure) have dissimilar solubility of elements [3,40,41]. In the results obtained in this work, we could identify small differences in the phase fractions of the ferrite and austenite phases between the grades 1.4662 (51% ferrite, 49% austenite) and 1.4462 (49% ferrite, 51% austenite), Table 4. This has likely contributed to the progress of attack within the materials, keeping in mind the preferential chromium partitioning in the ferrite phase.

4. Conclusions

In this paper, we have provided insights into the pitting corrosion of five stainless steels in dilute sulphuric acid in the presence of chlorides

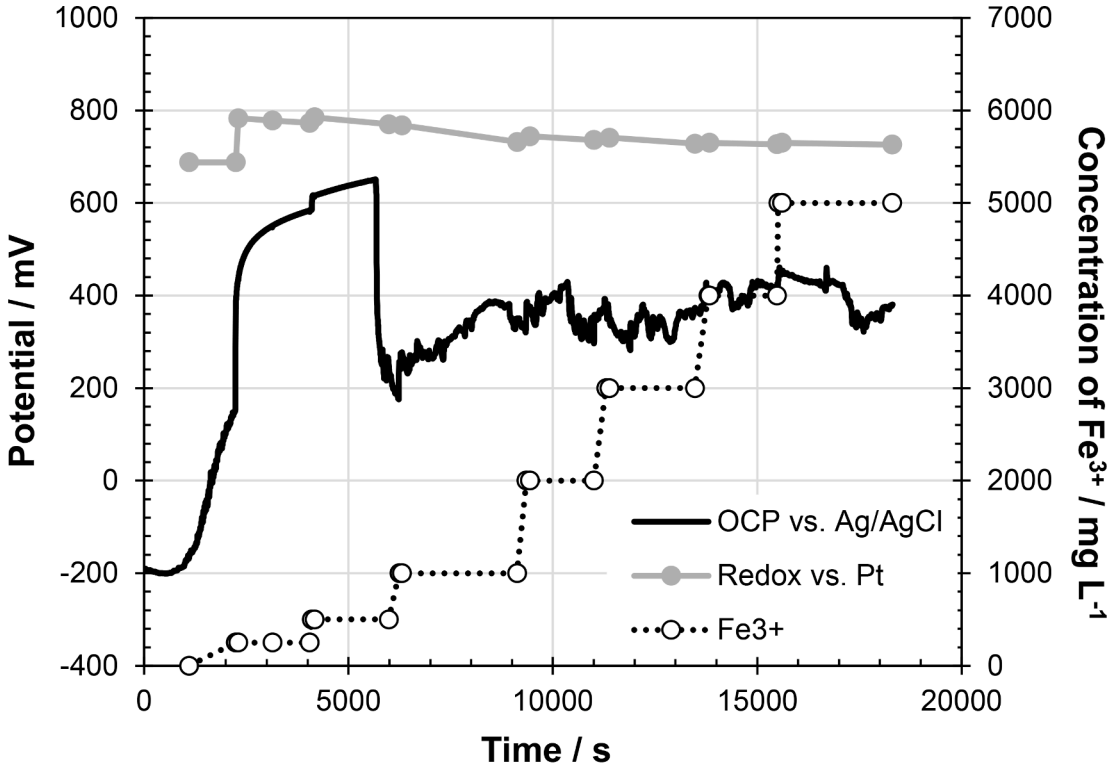

a)

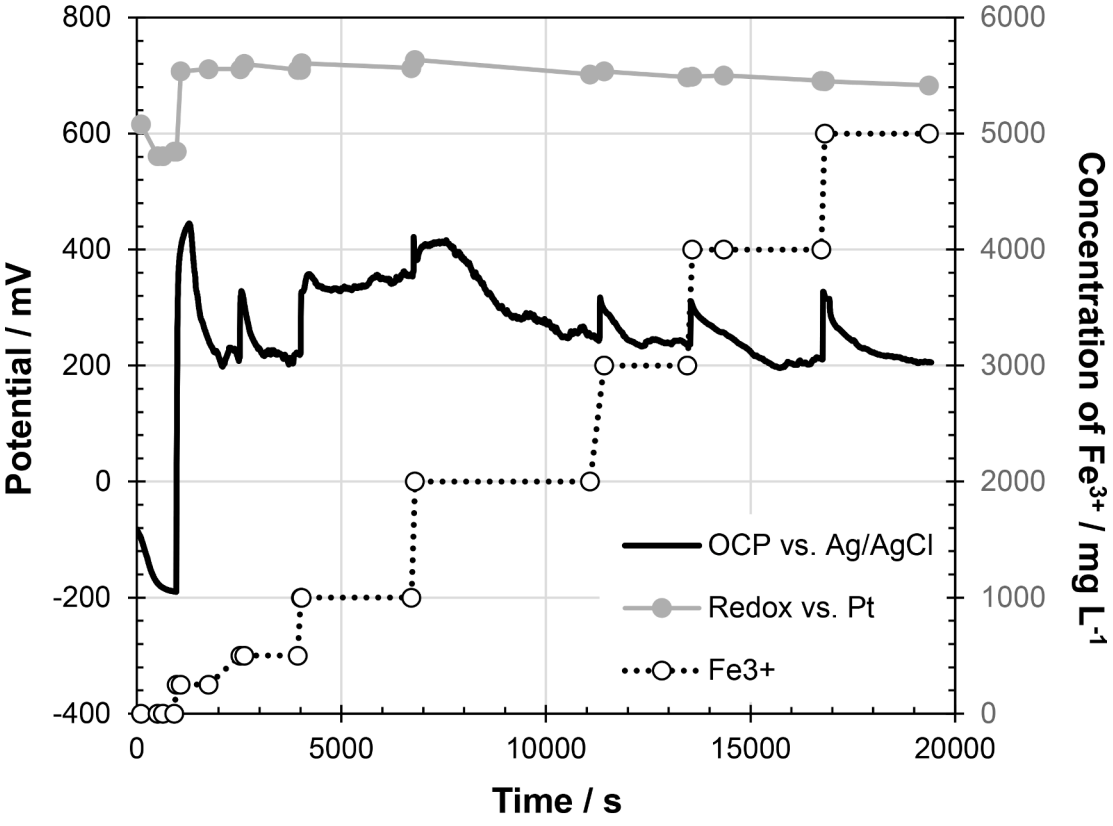

b)

Fig. 10. (*continued*).

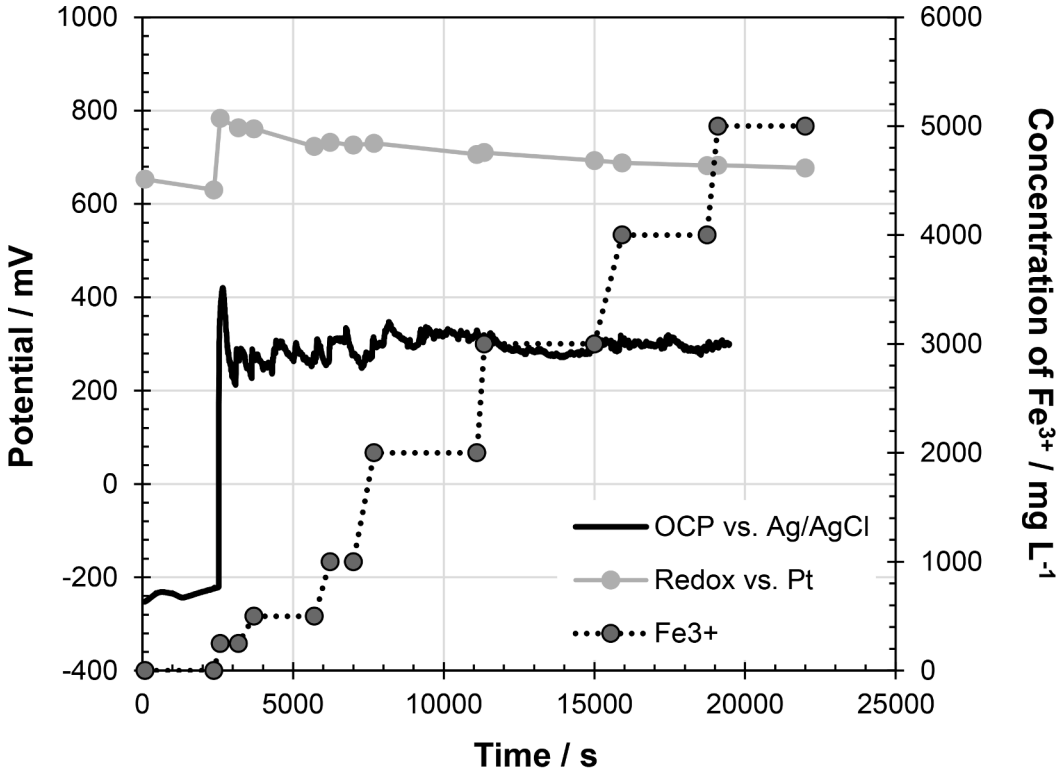

c)

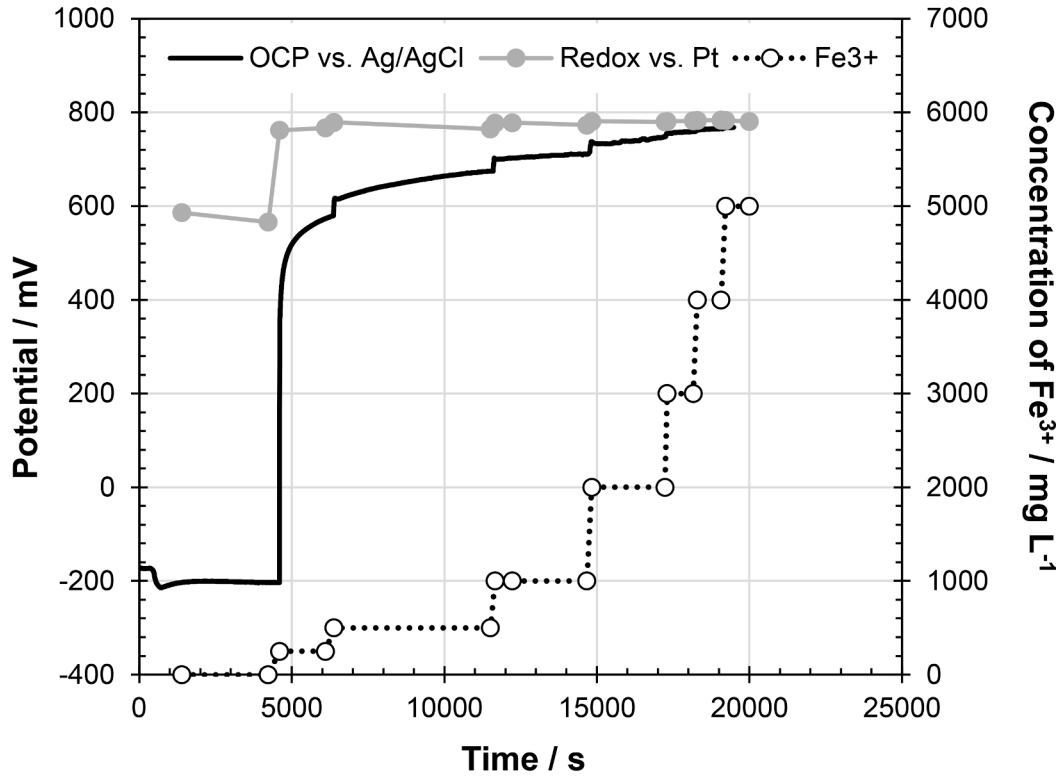

d)

Fig. 10. (*continued*).

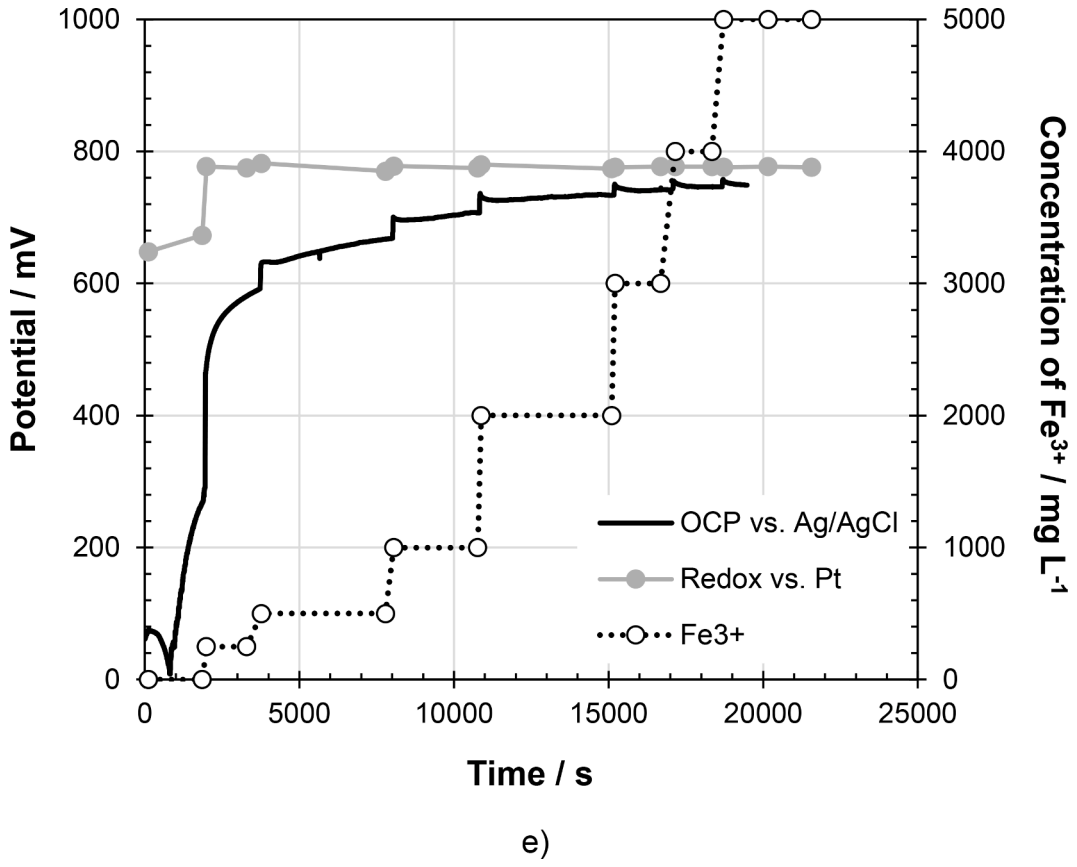

e)

Fig. 10. (*continued*).

by characterizing their microstructure, electrochemical behaviour at the temperatures of 50, 90 and 130°C, and susceptibility to pitting corrosion during 28-day immersion at 90°C. The test materials involved two austenitic and three duplex grades with the PRENs ranging from 33 to 44. The obtained results enable the following conclusions to be made:

- Most significant differences in the susceptibility of alloys to pitting corrosion could be detected at the temperature of 90°C. The temperature of 50°C was too low to induce pitting corrosion at the selected NaCl concentration range, while at the temperature of 130°C, the contribution by uniform corrosion via passive film dissolution grew in importance.
- amongst the lower-PREN (33–35) alloys, the two duplex grades: 1.4662 and 1.4462, were susceptible to pitting corrosion. Electrochemical measurements indicated pitting attack in the austenitic alloy 1.4539 (PREN 34), but it was not observed in immersion experiments. The two higher-PREN alloys, 1.4547 (PREN 43) and 1.4410 (PREN 44) were not susceptible to pitting corrosion as analysed by the used methods.
- In grade 1.4662, the pitting attack advanced preferentially in the ferrite phase, whereas it occurred primarily in the austenite phase of grade 1.4462. Compositional differences between the phases, in particular their nitrogen contents which have a radical influence on the PREN of the phase, explain the observations. Pitting attack in chloride-containing solutions occurred via passivity breakdown, which was seemingly facilitated by the presence of Fe^{3+} but not of Fe^{2+} or Cu^{2+} due to the higher oxidation capability of the former.
- No correlation between the chloride-to-sulphate activity ratio, $a(Cl-)/a(SO42-)$, and the susceptibility to alloys to pitting attack was found, in contrast to some earlier studies. This is likely due to the great overall resistance of the alloys to passivity breakdown due to their relatively high PREN values, making the adsorption of inhibitive species, i.e., the sulphate ion, less relevant than in the case of lower-PREN alloys. The addition of Fe^{3+} as ferric sulphate also changes $a(Cl^-)/a(SO_4^{2-})$, thus this one parameter is not enough to evaluate the aggressivity of complex electrolyte chemistries in hydrometallurgy.

CRediT authorship contribution statement

E. Huttunen-Saarivirta: Writing – review & editing, Methodology, Supervision, Project administration, Funding acquisition. **E. Isotahdon:** Investigation, Writing – review & editing. **Z. Que:** Investigation, Writing – review & editing. **M. Lindgren:** Writing – review & editing, Methodology, Supervision, Project administration, Funding acquisition. **A. Mardoukhi:** Investigation, Writing – review & editing. **J.-B. Jorcin:** Investigation, Supervision, Writing – review & editing. **P. Mocnik:** Investigation, Writing – review & editing. **T. Kosec:** Writing – review & editing, Methodology, Supervision, Project administration, Funding acquisition. **Y. El Ouazari:** Investigation, Writing – review & editing. **S. Hägg Mameng:** Investigation, Supervision, Project administration, Writing – review & editing. **L. Wegrelius:** Writing – review & editing, Methodology, Supervision, Project administration, Funding acquisition.

Declaration of Competing Interest

The authors declare the following financial interests/personal relationships which may be considered as potential competing interests:

Elina Huttunen-Saarivirta reports financial support was provided by EIT Raw Materials.

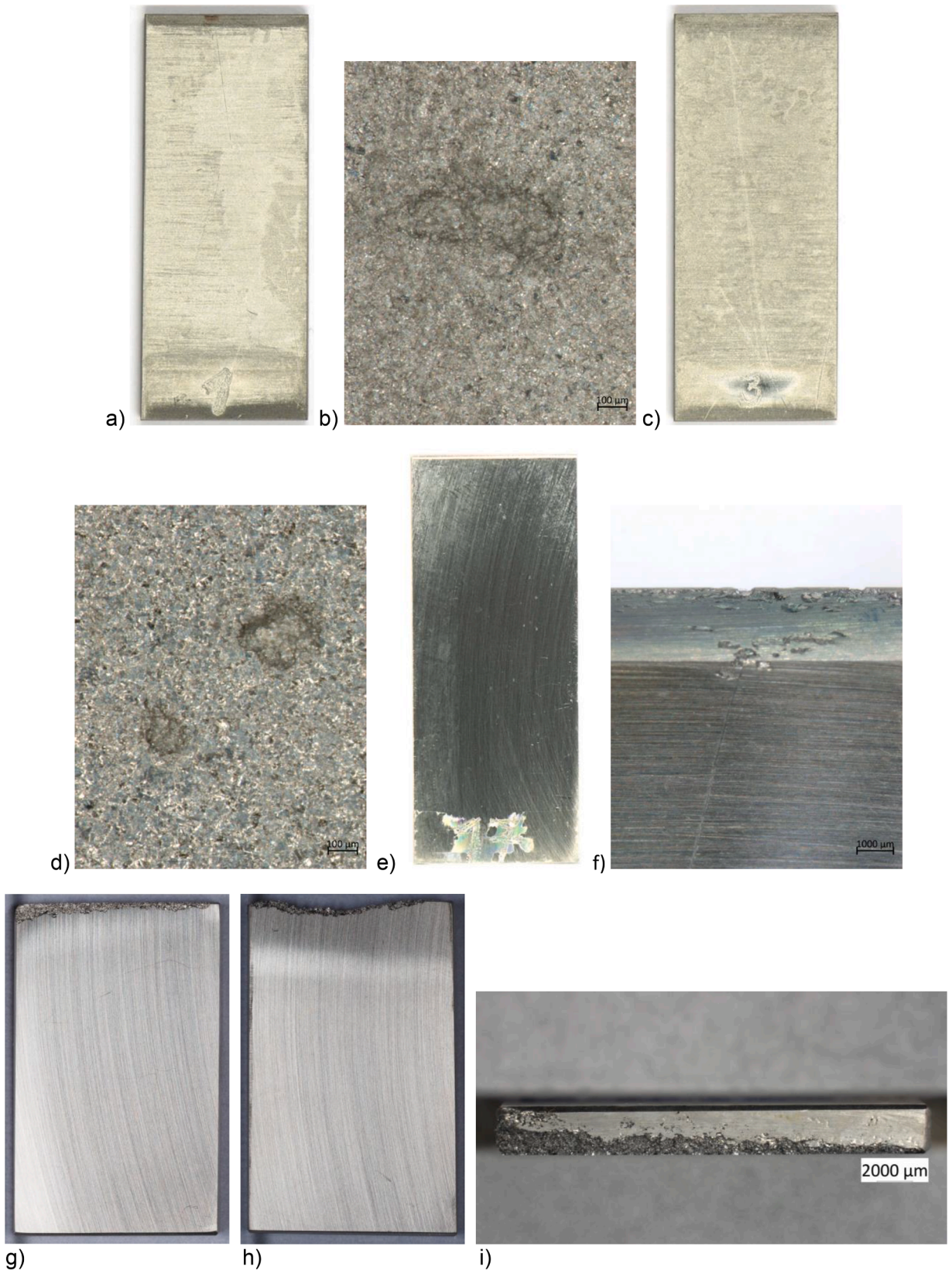

Fig. 11. Images of the specimens of austenitic grades 1.4539 (a-f) and 1.4547 (g-i) after the immersion experiment. a,b) Electrolyte #1. c,d) Electrolyte #2. e,f) Electrolyte #13. g-i) Electrolyte #19. a,c,e) and g-h) are photographs, while b,d,f) and i) are stereomicrographs.

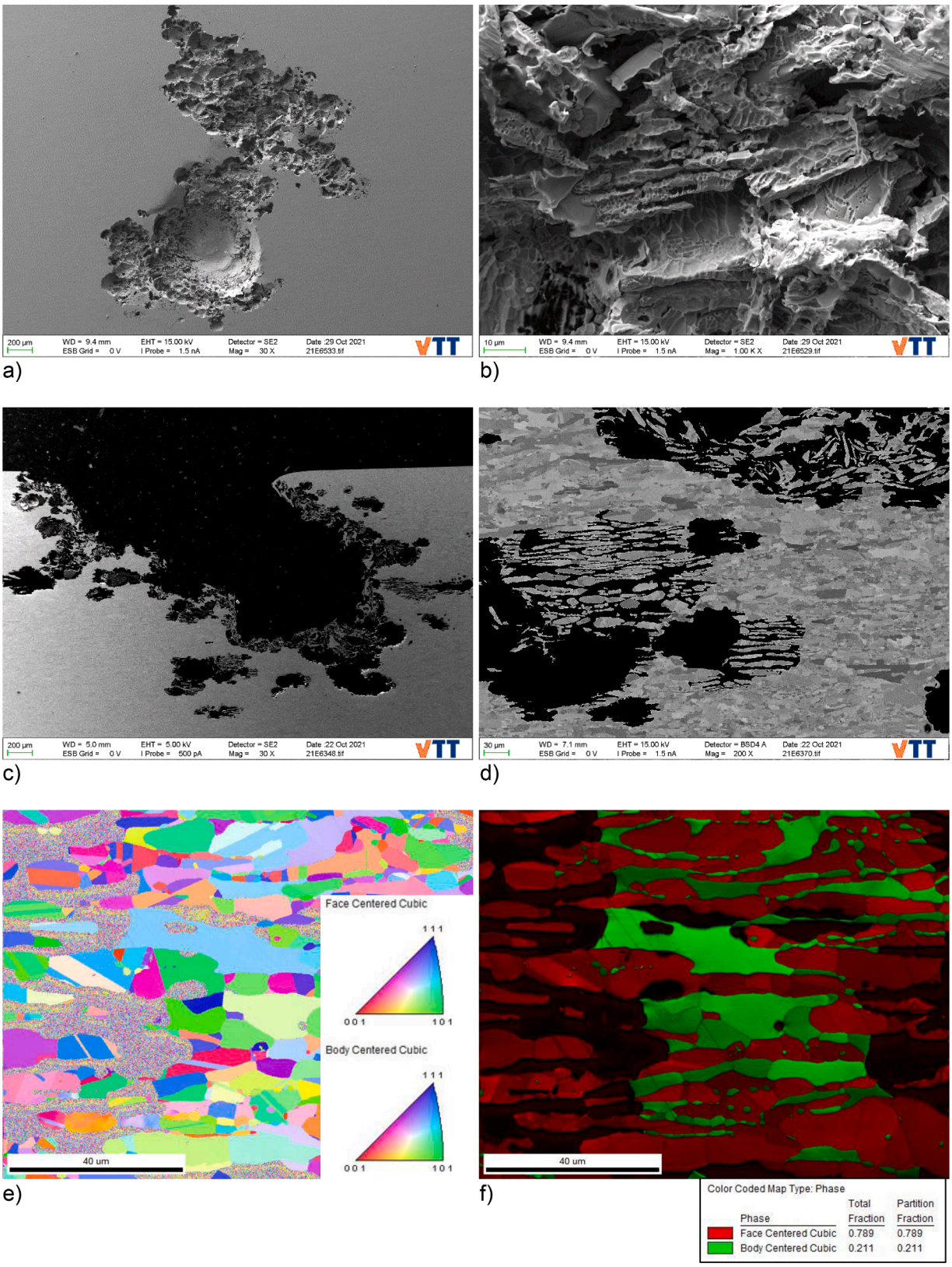

Fig. 12. SEM images, showing the progress of corrosion attack in the grade 1.4662. a,b) Plan view. c,d) Cross-sectional view. e) Crystallographic orientation of grains. f) Phase analysis, with red grains being austenite (FCC) and green grains being ferrite (BCC).

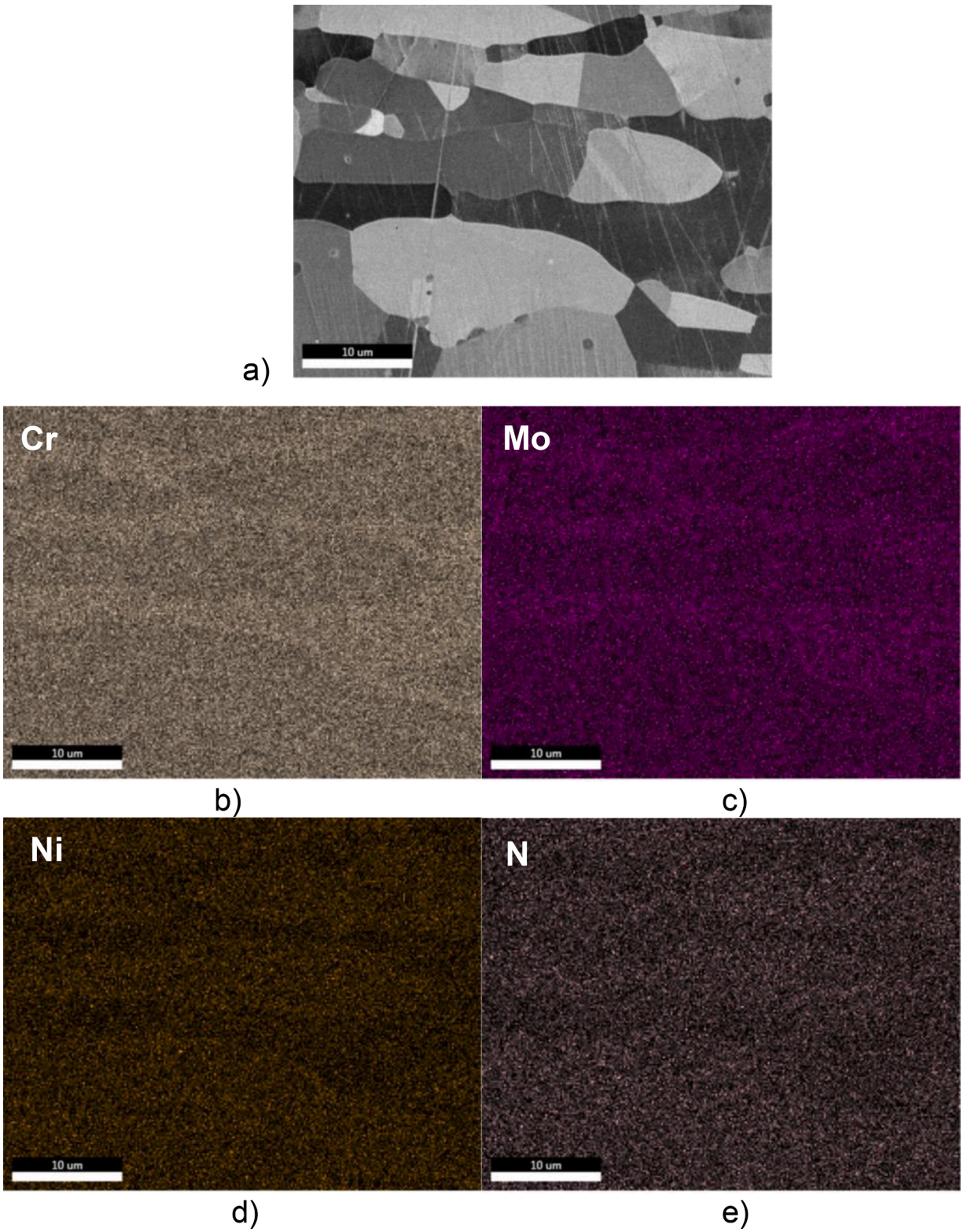

Fig. 13. a) SEM image and b-e) elemental maps of the grade 1.4662. b) Cr map. c) Mo map. d) Ni map. e) N map.

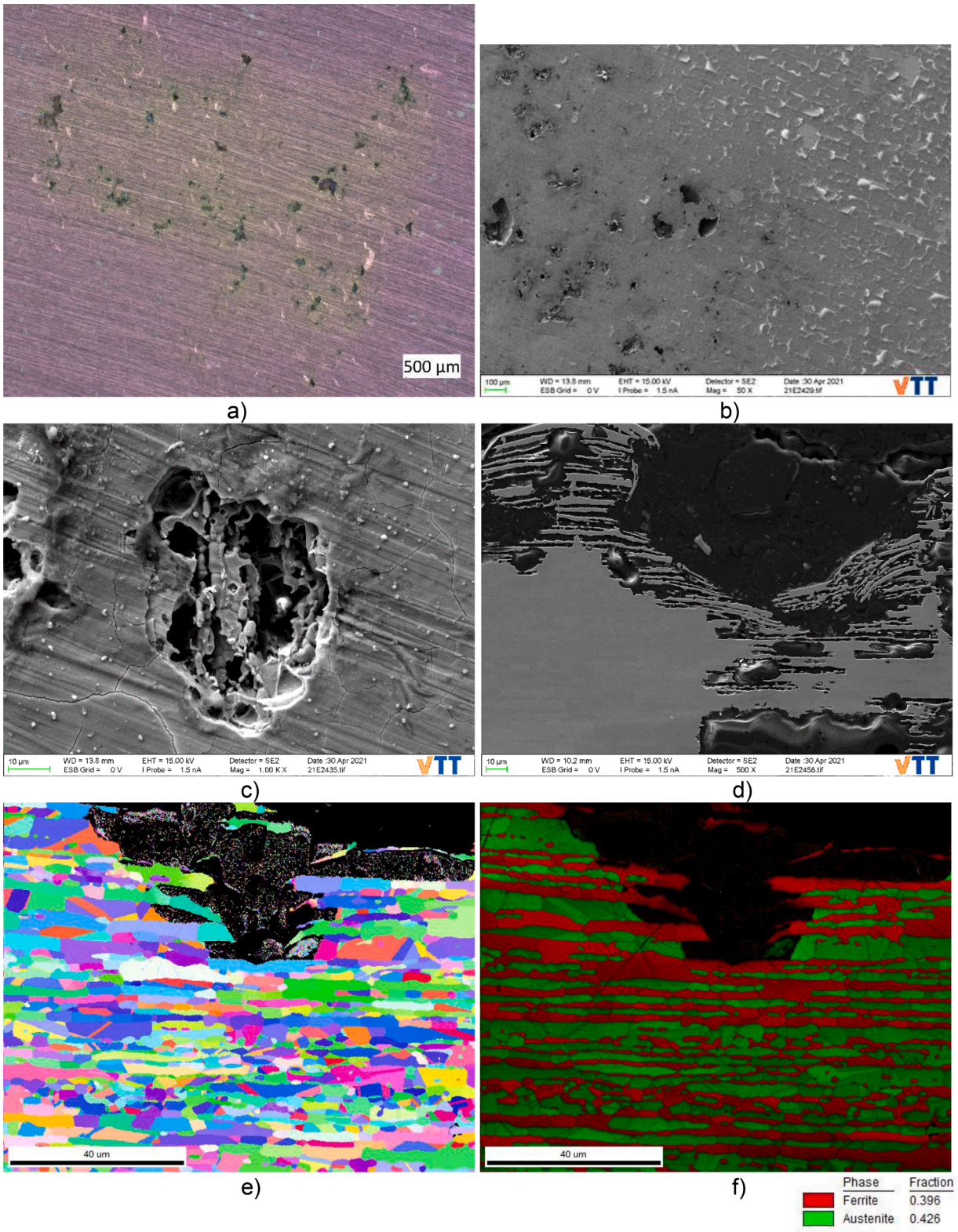

Fig. 14. a) Stereomicrograph and b-e) SEM images, showing the progress of corrosion attack in the grade 1.4462. a-c) Plan view. d) Cross-sectional view. e) Crystallographic orientation of grains. f) Phase analysis, with red grains being ferrite (BCC) and green grains being austenite (FCC).

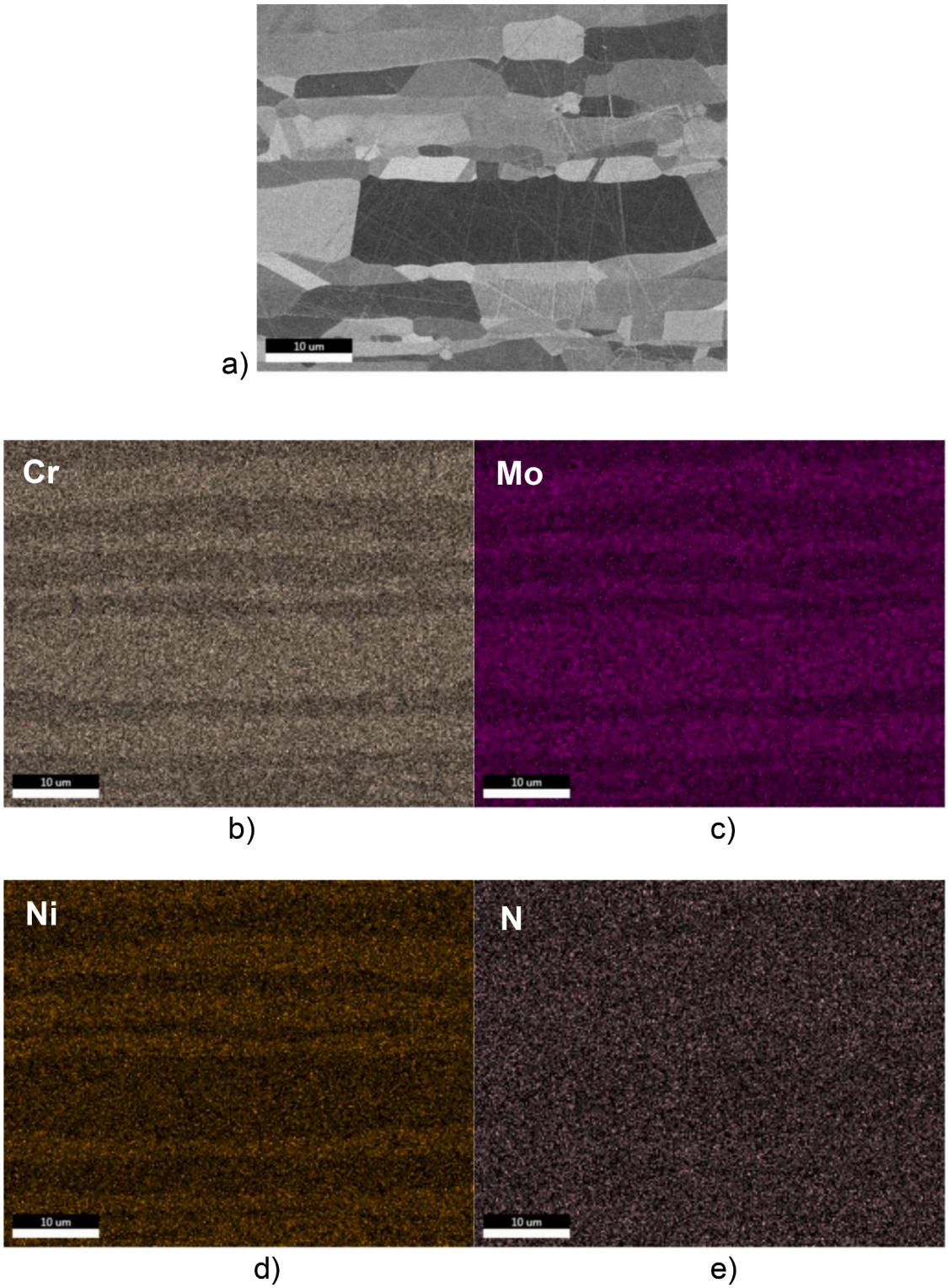

Fig. 15. a) SEM image and b-e) elemental maps of the grade 1.4462. b) Cr map. c) Mo map. d) Ni map. e) N map.

Data availability

Data will be made available on request.

Acknowledgements

The research has been funded by EIT Raw Materials (acceleration program, grant number 18158) and the partner organizations of the CORTOOLS project (2019–2021): VTT Technical Research Centre of Finland Ltd, Metso Outotec Finland Oy, ZAG Slovenian National Building and Civil Engineering Institute, Tecnalia, Outokumpu Stainless AB, Boliden Harjavalta Oy, Ferritico AB and Data Measuring Systems DMS. The funding is gratefully acknowledged.

References

[1] D.T. Llewellyn, R.C. Hudd, Stainless steels, in: D.T. Llewellyn (Ed.), Steels: Metallurgy and Applications, Butterworth-Heinemann, Oxford, UK, 1998.
[2] C.-O.A. Olsson, D. Landolt, Passive films on stainless steels –chemistry, structure and growth, Electrochim. Acta 48 (2003) 1093–1104.
[3] H.K.D.H. Bhadeshia, R.W.K. Honeycombe, Steels. Microstructure and Properties, Butterworth-Heinemann, Oxford, UK, 2003.
[4] E. Huttunen-Saarivirta, L. Kilpi, T.J. Hakala, L. Carpen, H. Ronkainen, Tribocorrosion study of martensitic and austenitic stainless steels in 0.01M NaCl solution, Tribol. Int. 95 (2016) 358–371.
[5] K. Eguchi, T.L. Burnett, D.L. Engelberg, X-Ray tomographic characterization of pitting corrosion in lean duplex stainless steel, Corros. Sci. 165 (2020), 108406.
[6] R.A. Bobadilla-Fazzini, A. Pérez, V. Gautier, H. Jordan, P. Parada, Primary copper sulfides bioleaching vs. chloride leaching: advantages and drawbacks, Hydrometallurgy 168 (2017) 26–31.
[7] G. Chauhan, P.J. Kaur, K.K. Pant, K.D.P. Nigam, Sustainable Metal Extraction from Waste Streams, Wiley-VCH Verlag GmbH & Co, Weinheim, Germany, 2020.
[8] L. Velasques Yévenes, H. Miki, M. Nicol, The dissolution of chalcopyrite in chloride solutions. Part 2: effect of various parameters on the rate, Hydrometallurgy 103 (2010) 80–85.
[9] H.R. Watling, Chalcopyrite hydrometallurgy at atmospheric pressure: 1. Review of acidic sulfate, sulfate-chloride and sulfate-nitrate process options, Hydrometallurgy 140 (2013) 163–180.
[10] J. van Yken, K.Y. Cheng, N.J. Boxall, A.N. Nikoloski, N. Moheimani, M. Valix, V. Sahajwalla, A.H. Kaksonen, Potential of metals leaching from printed circuit boards with biological and chemical lixiviants, Hydrometallurgy 196 (2020), 105433.
[11] M. Nicol, H. Miki, L. Velasquez-Yévenes, The dissolution of chalcopyrite in chloride solutions. Part 3. Mechanisms, Hydrometallurgy 103 (2010) 86–95.
[12] M. Lundström, J. Liipo, P. Taskinen, J. Aromaa, Copper precipitation during leaching of various copper sulfide concentrates with cupric chloride in acidic solutions, Hydrometallurgy 166 (2016) 136–142.
[13] G. Senanayake, A review of chloride assisted copper sulfide leaching by oxygenated sulphuric acid and mechanistic considerations, Hydrometallurgy 98 (2009) 21–32.
[14] S. Ekman, A. Bergquist, Suitable stainless steel grades for hydrometallurgical applications, in: Proceedings of the 6th International Symposium 2008, 2008, pp. 1038–1047.
[15] M. Lindgren, S. Siljander, R. Suihkonen, P. Pohjanne, J. Vuorinen, Erosion-corrosion resistance of various steel grades in high-temperature sulphuric acid solution, Wear 364-365 (2016) 10–21.
[16] M. Lindgren, R. Suihkonen, J. Vuorinen, Erosive wear of various stainless steel grades used as impeller blade materials in high temperature aqueous slurry, Wear 328-329 (2015) 391–400.
[17] M. Lindgren, E. Huttunen-Saarivirta, H. Peltola, J. Romu, T. Sarikka, H. Hänninen, P. Pohjanne, Crevice corrosion of stainless steels 904L, 2205, and 2507 in high-temperature sulfuric acid solution containing chlorides: influence of metal cations, Corrosion 74 (2018) 225–240.
[18] I. Ignatiadis, M. Amalhay, Experimental study of corrosion of two stainless steels during the oxidative bacterial dissolution of pyrite using mass loss and electrochemical techniques, Int. J. Miner. Process. 62 (2001) 199–215.
[19] Outokumpu Handbook of Stainless Steel, 2013.
[20] E. Huttunen-Saarivirta, E. Isotahdon, M. Lindgren, A. Mardoukhi, P. Mocnik, T. Kosec, J.B. Jorcin, S. Hägg Mameng, Y. El Ouazari, L. Wegrelius, Corrosion of stainless steels S31603, S31655 and S32101 in sulfuric acid solutions: effects of concentration, chlorides and temperature, Corrosion 78 (2022) 943–962.
[21] Z. Szklarska-Smialowska, Pitting and Crevice Corrosion, NACE International, Houston, USA, 2005.
[22] Z. Wang, A. Seyeux, S. Zanna, V. Maurice, P. Marcus, Chloride-induced alterations of the passive film on 316L stainless steel and blocking effect of pre-passivation, Electrochim. Acta 329 (2020), 135159.
[23] E. Altpeter, M.B. Rockel, Corrosion properties of high alloyed stainless steels in pure as well as in chloride containing sulphuric acid, Werkst. Korros. 34 (1983) 505–514.
[24] M.A. Streicher, General and intergranular corrosion of austenitic stainless steels in acids, J. Electrochem. Soc. 106 (1959) 161–180.
[25] N.J. Laylock, R.C. Newman, Temperature dependence of pitting potentials for austenitic stainless steels above their critical pitting temperature, Corros. Sci. 40 (1998) 887–902.
[26] C.T. Liu, J.K. Wu, Influence of pH on the passivation behaviour of 254SMO stainless steel in 3.5% NaCl solution, Corros. Sci. 49 (2007) 2198–2209.
[27] W.-.T. Tsai, M.-.S. Chen, Stress corrosion cracking behaviour of 2205 duplex stainless steel in concentrated NaCl solution, Corros. Sci. 42 (2000) 545–559.
[28] L.F. Garfias-Mesias, J.M. Sykes, C.D.S. Tuck, The effect of phase compositions on.
[29] https://www.mogroup.com/portfolio/hsc-chemistry/.
[30] ISO 18069: corrosion of metals and alloys. Method for determination of the uniform corrosion rate of stainless steels and nickel based alloys in liquids. 2015.
[31] https://thermocalc.com/.
[32] E. McCafferty, Introduction to Corrosion Science, Springer, New York, USA, 2010.
[33] X. Li, J.D. Henderson, F.P. Filice, D. Zagidulin, M.C. Biesinger, F. Sun, B. Qian, D. W. Shoesmith, J.J. Noël, K. Ogle, The contribution of Cr and Mo to the passivation of Ni22Cr and Ni22Cr10Mo alloys in sulfuric acid, Corros. Sci. 176 (2020), 109015.
[34] Handbook of Chemistry and Physics, 72nd Edition, CRC Press, Cleveland, USA, 1991.
[35] L.Q. Guo, M. Li, X.L. Shi, Y. Yan, X.Y. Li, L.J. Qiao, Effect of annealing temperature on the corrosion behaviour of duplex stainless steel studied by in situ technique, Corros. Sci. 53 (2011) 3733–3741.
[36] W.T. Tsai, J.R. Chen, Galvanic corrosion between the constituent phases in duplex stainless steel, Corros. Sci. 49 (2007) 3659–3668.
[37] B. Deng, Y. Jiang, J. Gong, C. Zhong, J. Gao, J. Li, Critical pitting and repassivation temperatures for duplex stainless steels in chloride solutions, Electrochim. Acta 53 (2008) 5220–5225.
[38] H. Yoon, H.-.Y. Ha, S.-.D. Kim, T.-.H. Lee, J.H. Jang, J. Moon, N. Kang, Effects of carbon substitution for nitrogen on the pitting corrosion resistance of type UNS S32205 duplex stainless steel, Corros. Sci. 164 (2020), 108308.
[39] Y.S. Lim, J.S. Kim, S.J. Ahn, H.S. Kwon, Y. Katada, The influences of microstructure and nitrogen alloying on pitting corrosion of type 316L and 20wt.% Mn-substituted type 316L stainless steels, Corros. Sci. 43 (2001) 53–68.
[40] H.-.Y. Ha, M.-.H. Jang, T.-.H. Lee, J. Moon, Interpretation of the relation between ferrite fraction and pitting corrosion resistance of commercial 2205 duplex stainless steel, Corros. Sci. 89 (2014) 154–162.
[41] H.-.Y. Ha, T.-.H. Lee, C.-.G. Lee, H. Yoon, Understanding the relation between pitting corrosion resistance and phase fraction of S32101 duplex stainless steel, Corros. Sci. 149 (2019) 226–235.